

5. Top of Deck Evaluation using Photogrammetry and Thermography

5.1 3DOBS at Near Highway Speed

3DOBS Near Highway Speed collected imagery at both demonstration bridges alongside the BridgeGuard thermal camera on the new mount. An image processing issue arose in the lab even though the imagery collected met all of the 3DOBS collection criteria (capture one lane per pass, correctly exposed and minimal motion blur). Agisoft software seemed to have issues correctly aligning the imagery and building the model. Even after adding in ground control points the resulting 3D model was warped and staggered.

The RED Epic camera was further tested under different conditions. These included both roadway and non-road features such as slopes. After successful reconstruction of other features, the demonstration bridges were reevaluated. Both Freer Rd and Maryland Ave were recently resurfaced and as a result they had very little variation in elevation on the surface. Tests conducted with slopes and other features which contained a significant variation in depth lead to successful reconstructions.

It was then determined that the reason for the inability to reconstruct the demonstration bridges was due to a lack of angular diversity between images because of the high quality (excellent condition) of deck surface. The Nikon D800 did not have this issue due to its higher resolution and ability to resolve smaller features. To prove this concept, another collection on Freer Rd. was made with the RED Epic. This time instead of driving one pass per lane, a third run was done down the middle of the bridge.

This third run down the middle was conducted to increase the overlap between all of the imagery. The effect would be that instead of a single feature only represented in at least five images in a single "flight line" (i.e., a driver over the bridge), it would also be represented in another flight line with at least five more images. The result is that there is greater than 100% overlap in the imagery, which would increase the chances of the software to correctly align the images and calculate depth (Figure 5-1 and Figure 5-2).

Using the new imagery from the Freer Road structure, Agisoft was able to correctly align the photos and create a DEM of the bridge deck. It confirmed that under situations where the bridge deck is in good conditions and contains very little or no distresses it is difficult to reconstruct 3DOBS outputs without additional imagery overlap. For bridges with significant spalls or other features, only a single pass per lane is needed, as there would be enough 3D information in the imagery for accurate reconstruction. Table 5-1 below is a table displaying the minimum distress sizes that 3DOBS Near Highway Speed can resolve.

Table 5-1: Minimum Resolvable Distresses for 3DOBS Near Highway Speed.

<i>System</i>	<i>Bridge Health Indicator</i>	<i>Minimum Size Resolved</i>	<i>Data Output Needed</i>	<i>Technique Used</i>
3DOBS Near Highway Speed	Spalls	1/8" depth and 1/2" wide	DEM	Visual or Automated Detection
	Cracking	1/8" wide	Orthoimagery	Visual
	Map Cracking	Spacing of 1/4"	Orthoimagery	Visual



Figure 5-1: Orthoimage of Freer Rd Generated from Imagery Collected from the RED Epic.

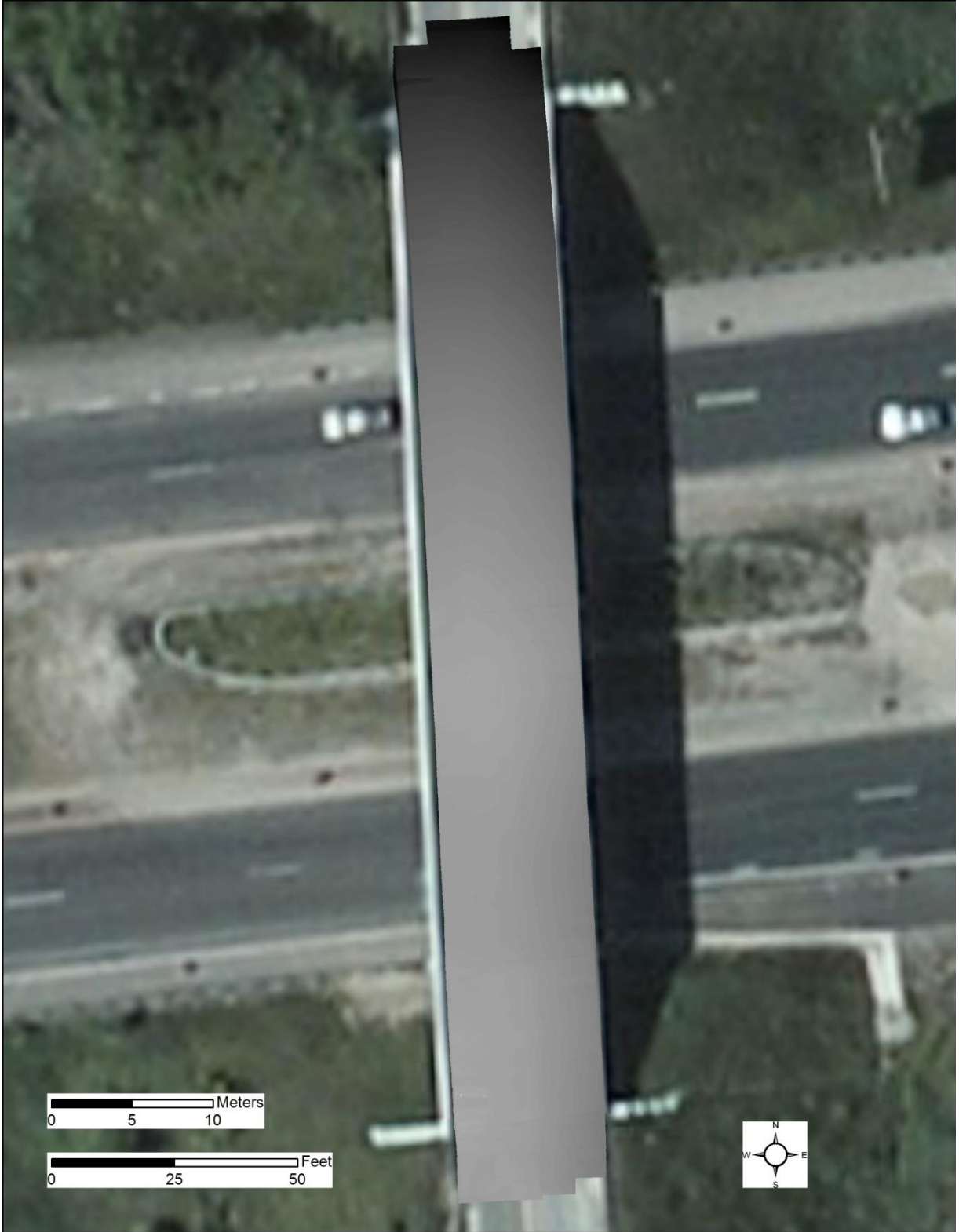


Figure 5-2: DEM of Freer Rd Generated from Imagery Collected from the RED Epic.

5.2 3DOBS High Resolution

The imagery collected from 3DOBS high-res was processed through Agisoft to generate an orthoimage, DEM and hillshade of Maryland Ave (Figure 5-3) and Freer Rd (Figure 5-5). The resulting x,y resolution of the Agisoft output is 0.5 mm and is shown in detail in Figure 5-4 and Figure 5-6.

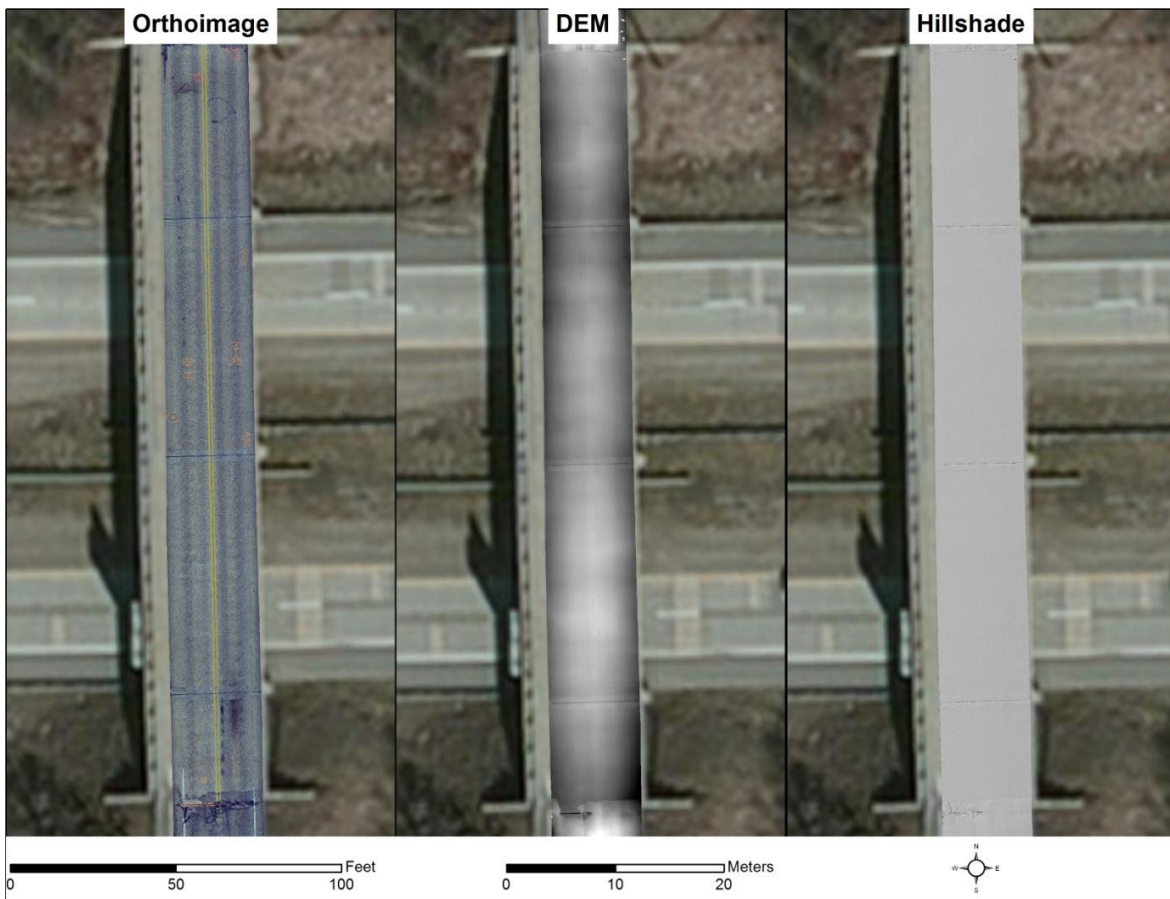


Figure 5-3: Overview of the Orthoimage, DEM and Hillshade Layers Generated from 3DOBS High Resolution over Maryland Ave.

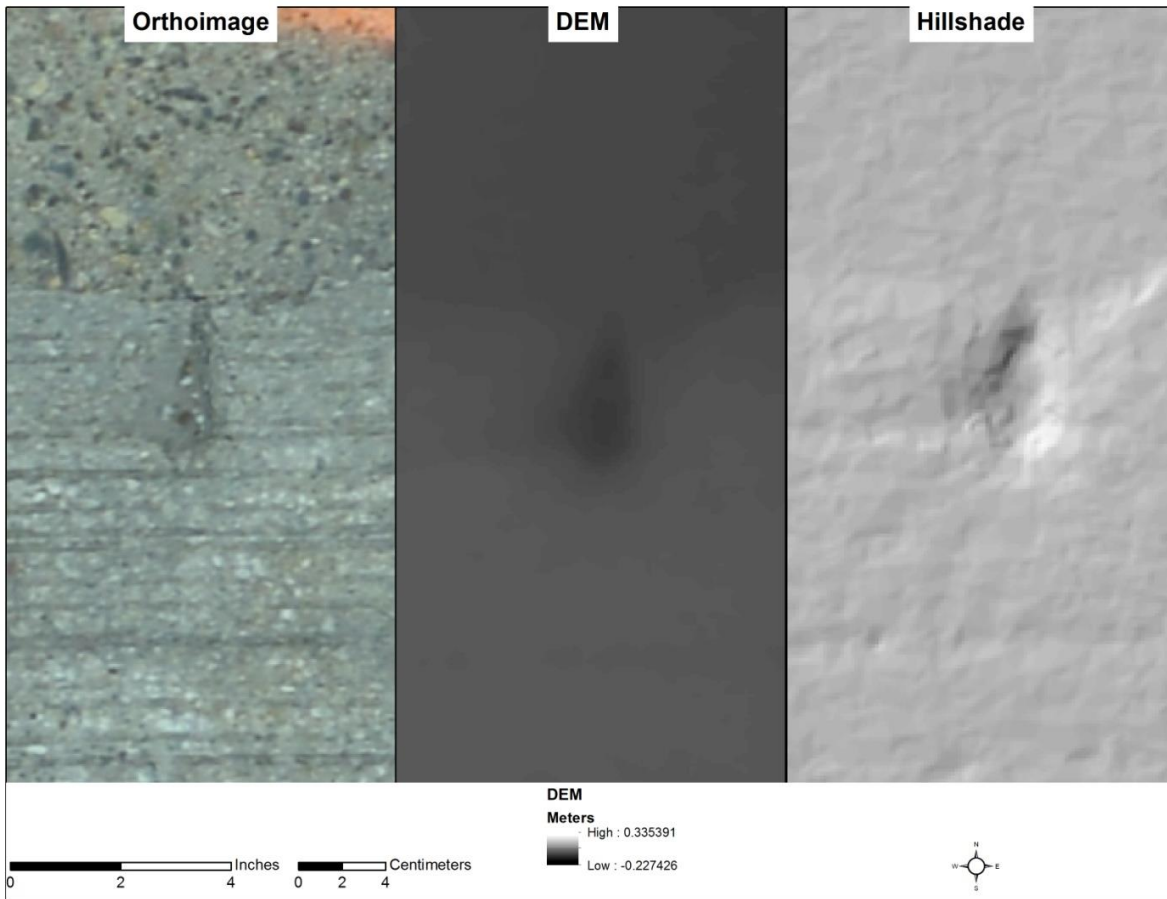


Figure 5-4: Zoomed In View of the Orthoimage, DEM and Hillshade Layers Generated from 3DOBS High Resolution over Maryland Showing 0.5 mm Resolution of the Outputs.

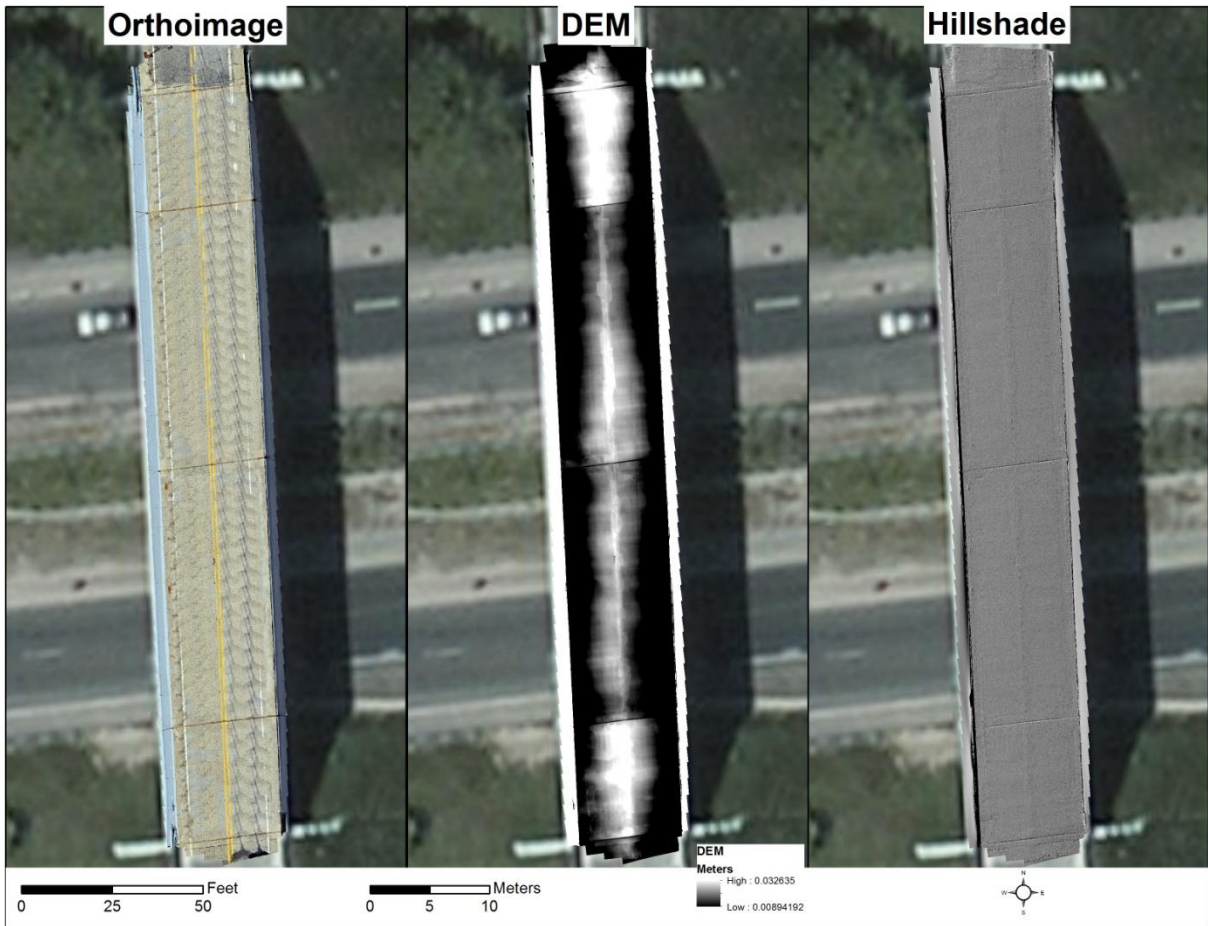


Figure 5-5: Overview of the Orthoimage, DEM and Hillshade Layers Generated from 3DOBS High Resolution over Freer Road.

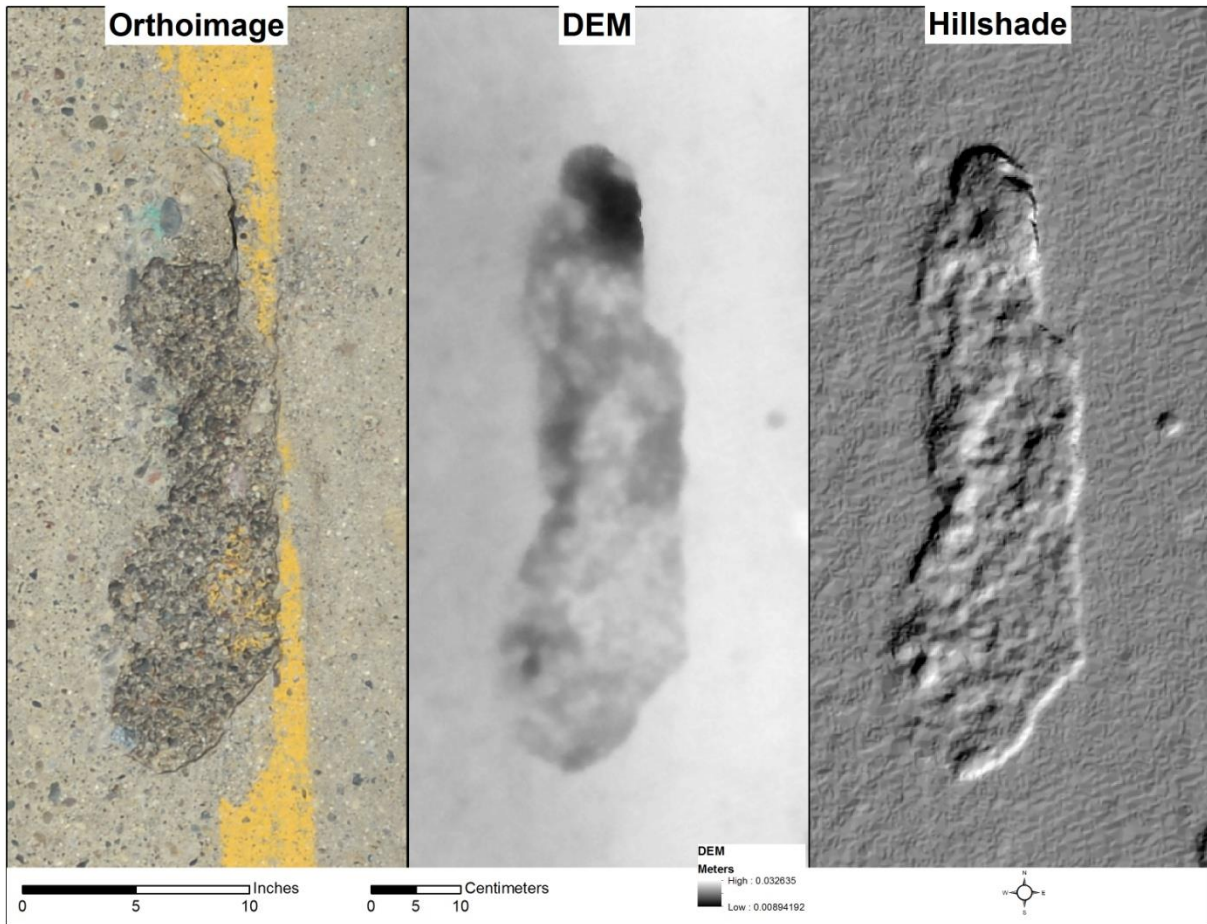


Figure 5-6: Zoomed in View of the Orthoimage, DEM and Hillshade Layers Generated from 3DOBS High Resolution over Freer Rd. showing 0.5 mm Resolution of the Outputs.

Crack detection was performed through visual inspection of the orthoimagery. With a resolution of 0.5 mm the smallest crack that could be seen is at least 1 mm or just over 1/32nd of an inch. Smaller cracks are not detectable since there needs to be at least two pixels over the crack in order for the crack to show in the imagery. For Maryland Ave (Figure 5-7) where MDOT marked some of the cracking, a visual inspection of the orthoimage located more cracking. Freer Rd also had some cracking but it was not marked by MDOT prior to the field data collection (Figure 5-8). Table 5-2 below is a table displaying the minimum distress sizes that 3DOBS High Resolution can resolve.

Table 5-2: Minimum Resolvable Distresses for 3DOBS High Resolution.

<i>System</i>	<i>Bridge Health Indicator</i>	<i>Minimum Size Resolved</i>	<i>Data Output Needed</i>	<i>Technique Used</i>
3DOBS High Resolution	Spalls	1/32" depth and 1/8" wide	DEM	Visual or Automated Detection
	Cracking	1/32" wide	Orthoimagery	Visual
	Map Cracking	Spacing of 1/16"	Orthoimagery	Visual



Figure 5-7: Detected Cracks on Maryland Ave.

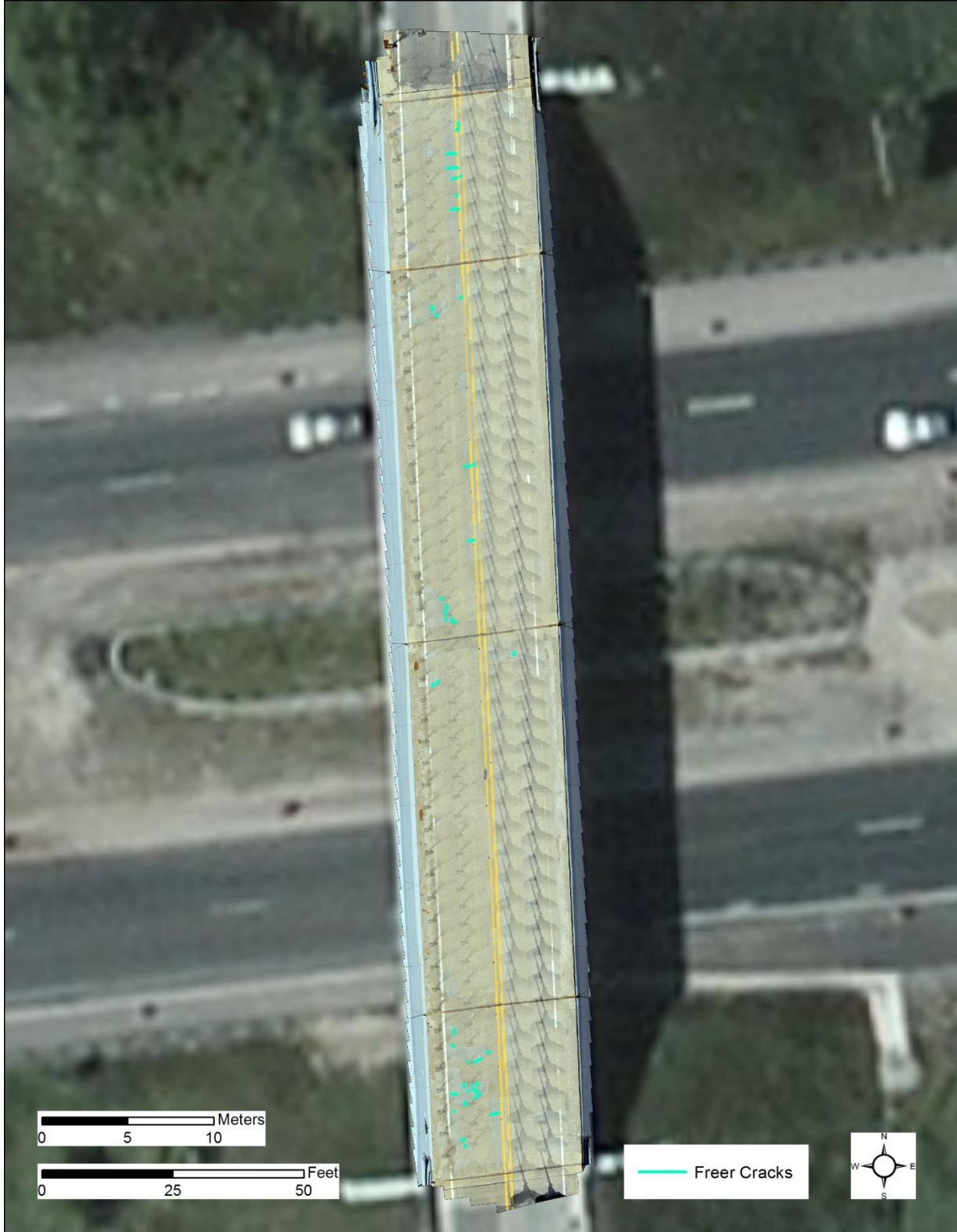


Figure 5-8: Detected Cracks on Freer Rd.

5.3 BridgeGuard Passive Infrared Thermography

During the analysis phase, the delaminations and spalls were identified, quantified and percentages obtained, based on total square foot area. The results are comprehensive and assembled in a manner that can be easily incorporated into Inspection Reports, Pontis, work recommendations, and/or detailed scoping documents. Appendix B-F includes the individual reports for the bridge decks evaluated in this study.

All reports and deliverables are designed to meet the needs, requirements, and expectations of the client and can be submitted in MicroStation or AutoCAD native files with MS Excel spreadsheets summarily detailing the locations and sizes of defects, and are subject to QA/QC reviews prior to being submitted.

During the field testing phase, BridgeGuard assessed bridge decks separately from 3DOBS. Figure 5-9 shows BridgeGuard results from 20 Mile Rd. and it was determined that there was 1,767 ft² of potential delaminations on the bridge deck. This was almost 500 ft² more than was recorded by MDOT. For 24 Mile Rd. BridgeGuard determined that there was 1,765 ft² of potential delaminations on the bridge deck (Figure 10). Compared to MDOT, this was approximately 1,000 ft² more than MDOT's estimate.

US-131 consists of two bridges, each with its own report. For the north bound lanes the BridgeGuard assessment determined there was 1,609 ft² of potential delaminations (Figure 11). The south bound lanes contained 989 ft² of potential delaminations according to BridgeGuard's analysis (Figure 12). By comparison MDOT reported there was 2,072 ft² for the north bound lanes and 759 ft² for the south bound lanes.

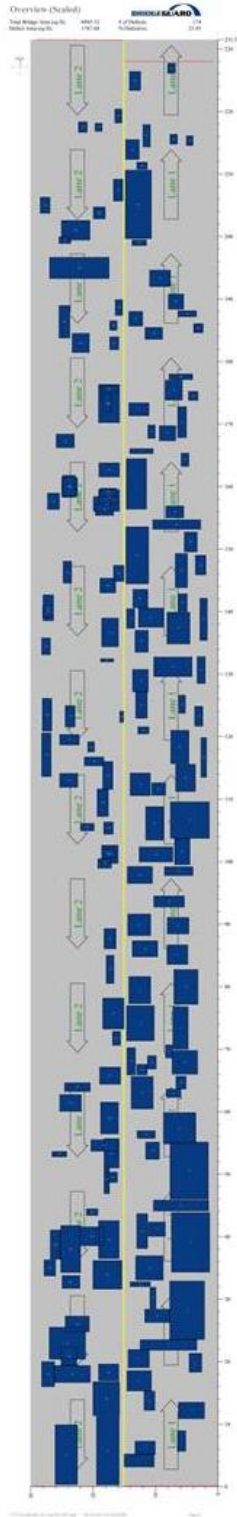


Figure 5-9: Location of Potential Delaminations as Determined by BridgeGuards Thermal Survey on 20 Mile Rd.

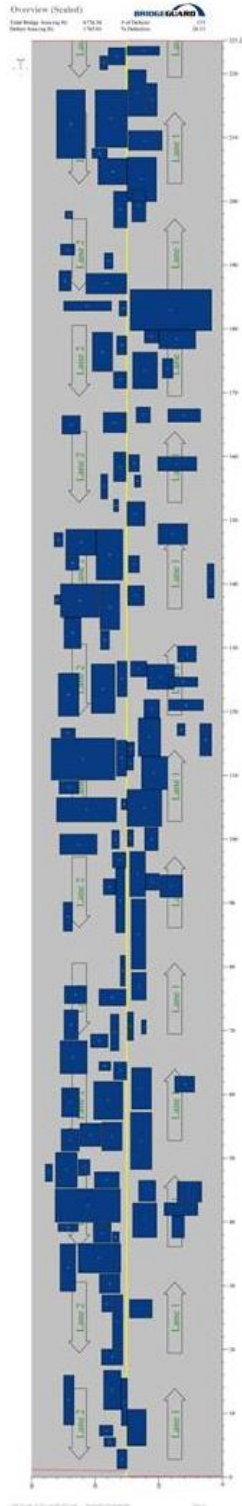


Figure 5-10: Location of Potential Delaminations as Determined by BridgeGuards Thermal Survey on 24 Mile Rd.

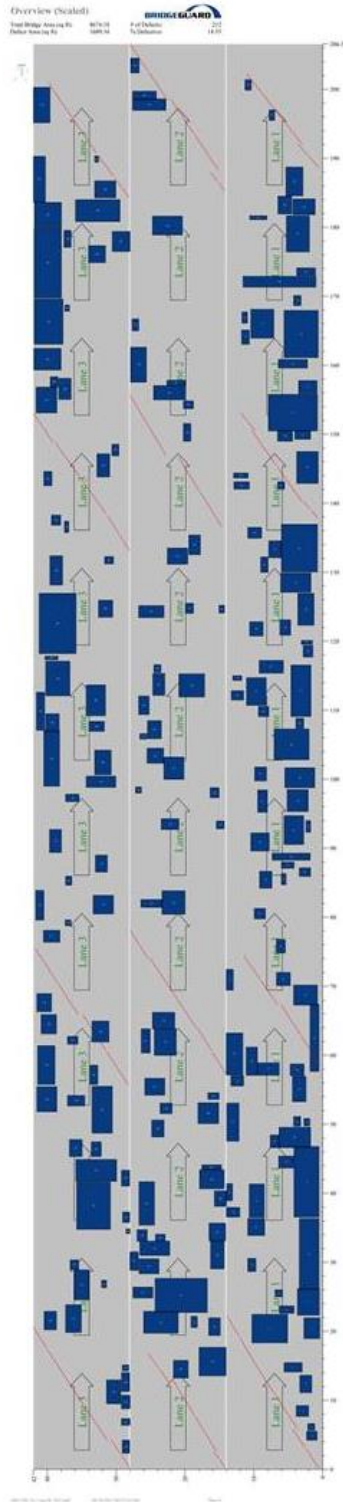


Figure 5-11: North Bound Lanes of US-131 Showing Potential Delaminations from the BridgeGuard Survey.

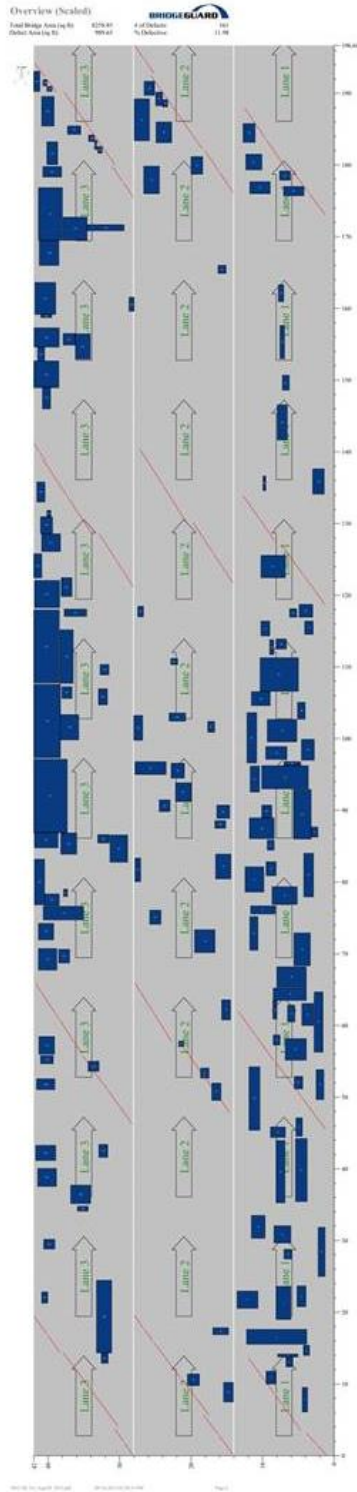


Figure 5-12: South Bound Lanes of US-131 Showing Potential Delaminations from the BridgeGuard Survey.

5.4 BridgeViewer

Imagery collected with BridgeViewer was geotagged using the track log from the GPS used in the vehicle. The geotagging process produces a shapefile of the picture locations as well as watermarked pictures that include the Lat/Lon and date/time (Figure 5-13). The imagery from the two cameras was also separated into right and left as they were mounted (Figure 5-14). Because there was only one GPS, the photos were tagged to the center of each lane. The shapefile is then edited to separate the right and left cameras to represent the offset as they were collected.

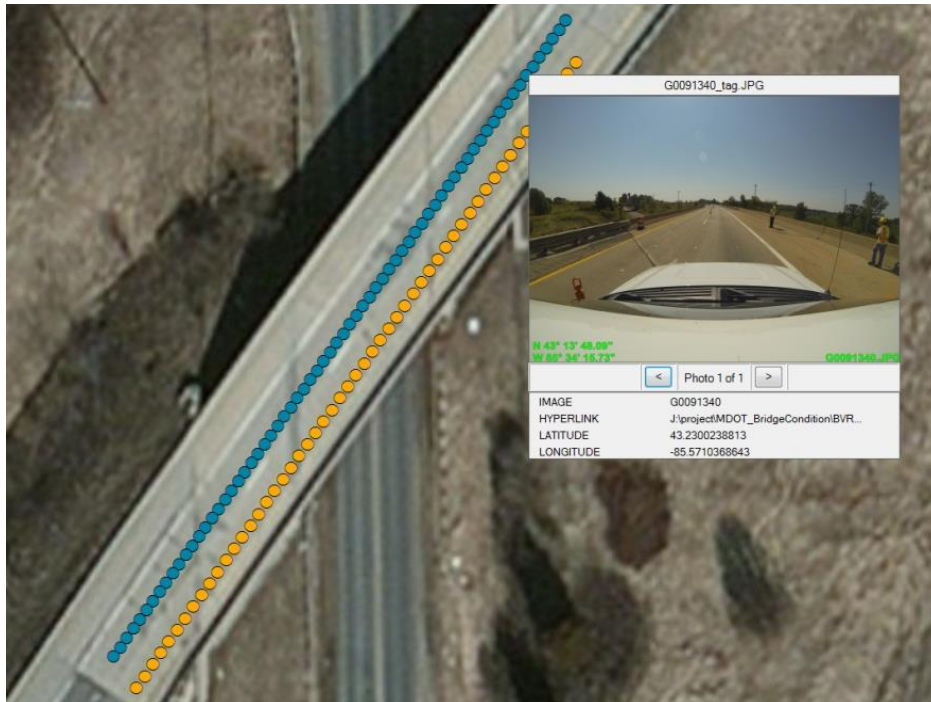


Figure 5-13: BridgeViewer Collect on US-131 near Grand Rapids, MI. For this Collect the Cameras were Mounted to the Roof of the Vehicle since the Hood was not Steel.

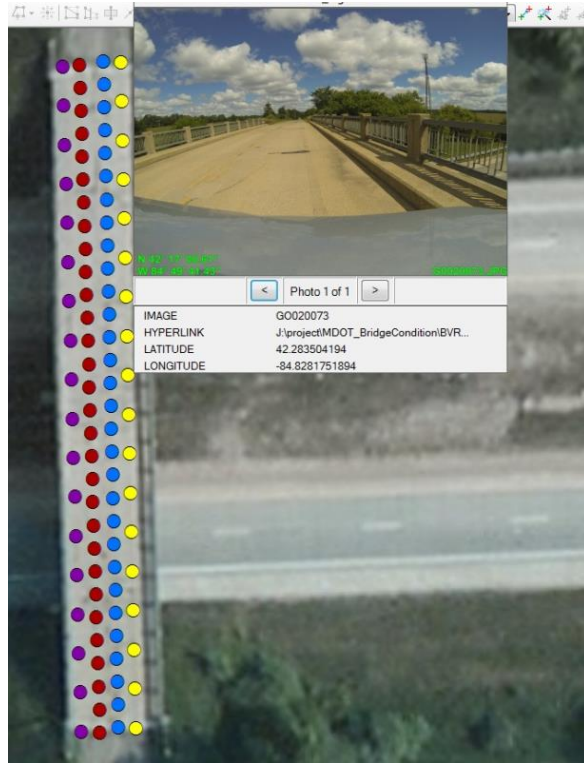


Figure 5-14: BridgeViewer collect of 24 Mile Rd near Marshall, MI.

5.5 System Integration Results

After the data are collected, a spall detection analysis is run for 3DOBS, a delamination detection is performed by BridgeGuard for the thermal the imagery, and results are combined within ArcMap GIS software. 3DOBS data and results are already generated as GIS layers and shapefiles with a geographic reference. BridgeGuard data is not referenced in a standard GIS format but it is locally referenced to the bridge.

The thermal images collected by BridgeGuard are individually georeferenced to the orthoimage created by 3DOBS. This is done using the georeferencing tool in ArcMap. Once georeferenced they are mosaicked (using the ArcGIS “mosaic to new raster” tool) to form a single image (tif) layer that can be easily displayed in any GIS. The detected delaminations are then traced in ArcMap to create a separate shapefile (Figure 5-15).

The final GIS output for a bridge includes six layers: an orthoimage, DEM, Hillshade, thermal layer, detected spalls shapefile, and delaminations shapefile. As noted by MDOT Survey Support staff, another useful geospatial layer can be created – a 3D point cloud in standard LAS format that can be analyzed and visualized using image processing software. The shapefile of detected cracks is also spatially referenced similar to the spalls layer except it is only produced from the high-res version of 3DOBS. All of these data sets overlay in a GIS, which makes it easy to

analyze spalls and delaminations simultaneously (Figure 5-16). Spalls and delaminations can easily be visualized while overlaid on the orthoimage or the thermal layers (Figure 5-17).

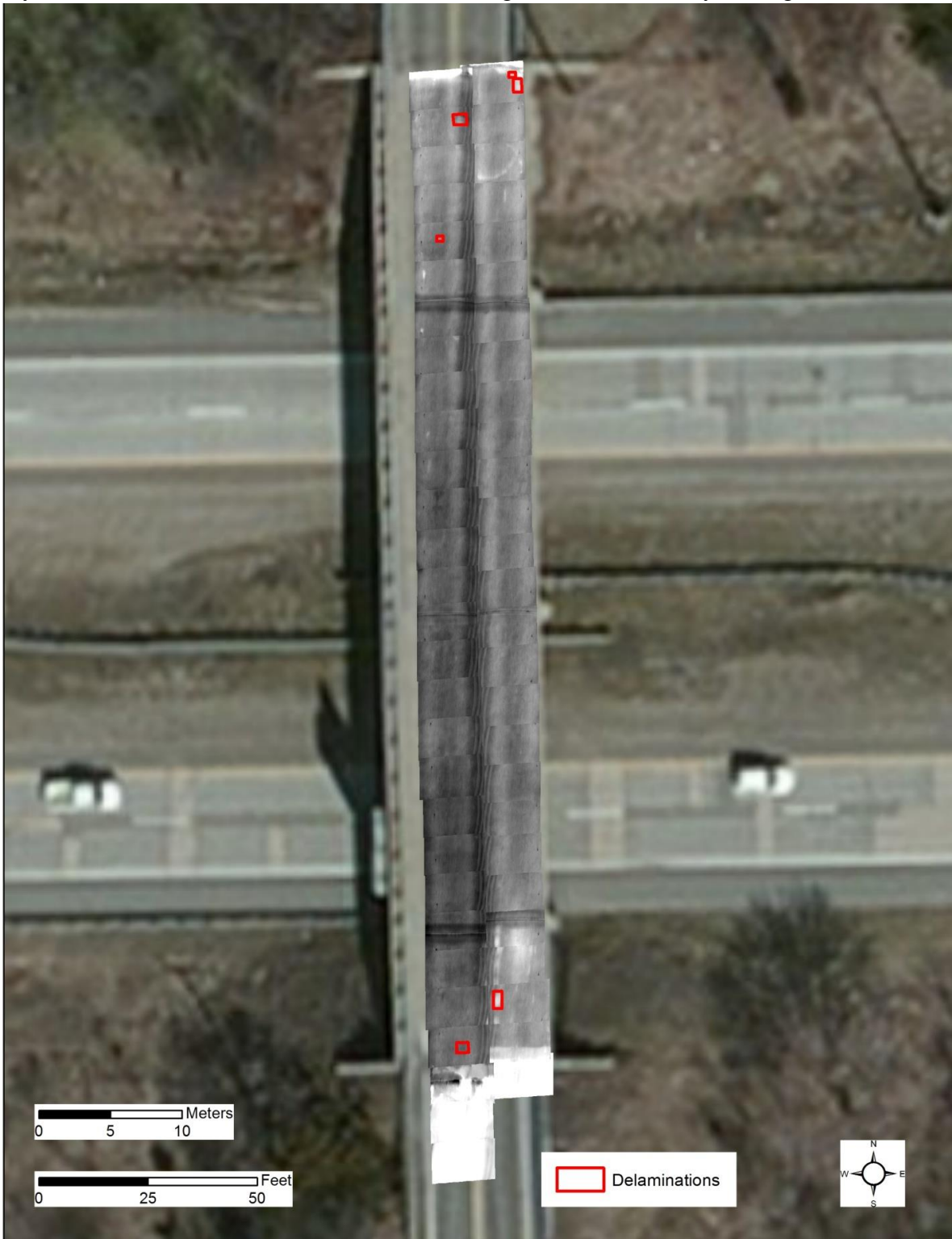


Figure 5-15: BridgeGuard Imagery as Georeferenced Layers with Delaminations Shapefile.

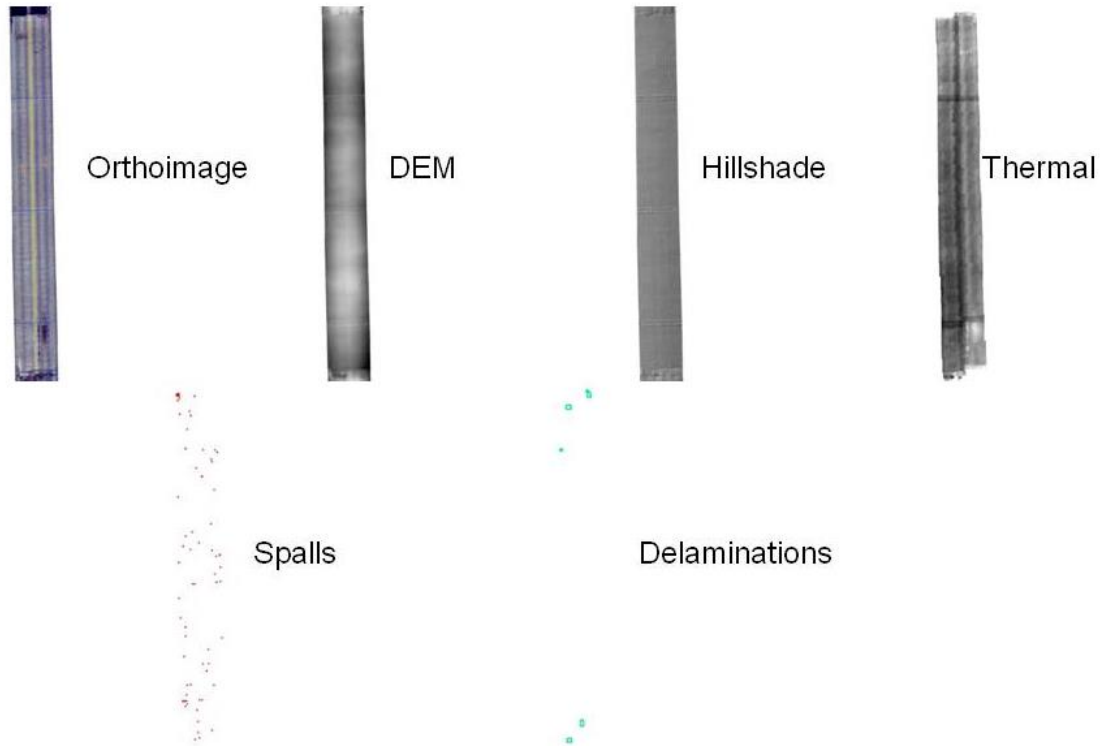


Figure 5-16: All of the Data Sets Created from the Combined System.



Figure 5-17: Comparison of the Results Generated from 3DOBS High Speed and the BridgeGuard Thermal Cameras as a Combined System over Maryland Ave.

Through the combination of these technologies, bridge inspectors are able to visualize and objectively assess the surface and subsurface condition of concrete bridge decks. All of the output generated is in the form of GIS layers and shapefiles that can be viewed in any GIS. Once in a GIS, these files can be processed using a variety of tools to extract more information out of the optical and thermal data collected. One example would be if multiple collects are done over a period of time, a change detection analysis can be performed and deterioration rates can be calculated.

6. Underside of Deck Evaluation using Active Infrared Thermography

Non-destructive testing (NDT) techniques have shown potential in accurately assessing the deterioration condition of concrete bridge elements but few have the capabilities needed to quantify subsurface defects such as delaminations. However, these technologies are not readily deployable during routine bridge inspections. Infrared thermography is one remote sensing NDE technique that is gaining popularity among bridge inspectors due to its potential in detecting delaminations within concrete structural elements and its simplistic method of data acquisition and analysis. Infrared thermography can be conducted in either a passive or active test set-up. Active infrared (IR) thermography can overcome some obstacles associated with passive infrared thermography due to the use of an external heating source, rather than relying on solar energy and the presence of the sun. Although more focus in the bridge inspection field is given to passive infrared thermography inspection (ASTM 2007), active infrared thermography also has capabilities for detecting delaminations specifically on structural elements found on the underside of bridges that are not exposed to direct sunlight (Vaghefi 2001).

A primary objective was to determine the feasibility of using active IR thermography for detecting delaminations on the deck underside and fascia beams. Through a series of laboratory tests, the active heating method was investigated to include variable depth delaminations and heating time. A proof of concept field demonstration confirmed the feasibility of using active IR thermography for concrete delamination detection on an in-service bridge in areas not exposed to passive solar heating. Testing was conducted on a bridge located in downtown Grand Rapids, Michigan and provided valuable information regarding the current condition of the underside of the bridge deck and side of a pier cap. A simple method to quantify suspected delamination area is defined to evaluate performance of the active IR method. This chapter provides a comprehensive evaluation of active thermal IR for deck inspection including laboratory and field demonstration results leading to recommendations for further development prior to implementation.

6.1 Active Thermography for Concrete Bridge Element Evaluation

Unlike passive infrared thermography, active IR thermography involves a transient heat transfer phenomena using an external heater other than the sun or thermal properties of the object itself. In this case, electromagnetic energy is transmitted to the specimen by an external heater and radiant energy emitted from the object can be recorded using a thermal infrared camera. This testing procedure requires that the specimen be intentionally heated to create a gradient temperature difference between the object's interior and surface. As infrared radiation from the heater propagates through dry concrete, delaminations restrict the heat transfer and the concrete near the surface retains more heat than surrounding areas of sound concrete. Thermal IR images are collected during either the heating or cooling period.

A variety of controllable heating sources, including hot air guns, quartz lamps and heat blankets can be used to produce thermal excitation on the test specimen. Active IR thermography techniques are commonly named based on the source of the external heater. Examples of active methods include: Pulsed (Flash) thermography, Pulsed phase thermography, Lock-in thermography, Vibrothermography, Inductive thermography, Laser spot thermography and Step heating (Maldague 1993). This study specifically focused on pulsed thermography with pulse heating times of 5 and 15 minutes.

6.1.1 Advantages of Bridge Inspection Using Active Infrared Thermography

Similar to passive infrared thermography, the capability of detecting subsurface defects and delaminations, commercial availability, remote sensing, ease of data collection and image interpretation are some of the benefits of using the active IR thermography technique for bridge inspection. Remote data collection of active IR thermography is an outstanding advantage of this technology, which helps in reducing traffic disruption and lane closures during the testing period. With the ability to store data for monitoring the damage growth process during the service life of a structure, condition assessments using active IR thermography also allow for better allocation of bridge maintenance funds.

Determination of delamination depth, as well as the location and size, is an important feature in active infrared thermography (Maldague 1993). This approach is not dependent on the weather condition and clear sky; therefore, it allows conducting a bridge inspection in a larger time window during the day. Furthermore, this method can be applied on the concrete bridge elements which are not exposed to the direct sunlight, such as girders and the underside of the bridge deck.

6.1.2 Limitations of Bridge Inspection Using Active Infrared Thermography

Although active IR thermography allows for a wider inspection time window and does not have to be conducted at a certain time of day, environmental conditions can impact the data collection process, such as moisture on the test surface from precipitation or condensation.

Materials with different emissivity on the surface (for example patched areas surrounded by existing concrete) provide challenges in detecting subsurface flaws due to the perturbing contrast in thermal infrared images. As with passive IR thermography, optical (visual) images are recommended (Vaghefi and Ahlborn 2013).

6.2 Laboratory Experiment Methodology

To investigate the feasibility of using active IR thermography to detect and quantify delaminations in concrete test specimens, a laboratory test set-up was developed following an in-depth literature review of this non-destructive remote sensing condition assessment technique.

Several laboratory experiments were conducted using the concrete test specimens, equipment, procedure, and analysis methods described in the following sections.

6.2.1 Concrete Test Specimens

As layers of concrete separate and delaminations form, pockets of air become present within the concrete. Due to the difference in thermal conductivity of concrete and air, these subsurface defects can be detected using a thermal infrared camera when exposed to a thermal impulse. To simulate the presence of delaminations in concrete, a material with similar thermal properties to air was selected and embedded into several concrete specimens. Due to the similarity of the thermal conductivity between air and Styrofoam with respect to concrete, 3/8 in. thick Styrofoam blocks were selected to simulate delaminations (Vaghefi 2013). The thermal conductivity of air was determined to be $0.024 \text{ W}/(\text{m}^\circ\text{K})$ or $0.116 \text{ (Btu x in)}/(\text{hr x ft}^2 \text{ x }^\circ\text{F})$ while the conductivity of Styrofoam was determined to be $0.03 \text{ W}/(\text{m}^\circ\text{K})$ or $0.229 \text{ (Btu x in)}/(\text{hr x ft}^2 \text{ x }^\circ\text{F})$ (Maldague 1993; Engineering ToolBox 2012). With the thermal conductivity of dry concrete being between 0.4 and $1.8 \text{ W}/(\text{m}^\circ\text{K})$ or 2.8 and $12.5 \text{ (Btu x in)}/(\text{hr x ft}^2 \text{ x }^\circ\text{F})$, Styrofoam can be considered representative of delminations within concrete elements (Lamond and Pielert 2006).

6.2.1.1 Laboratory Test Slabs I-VI

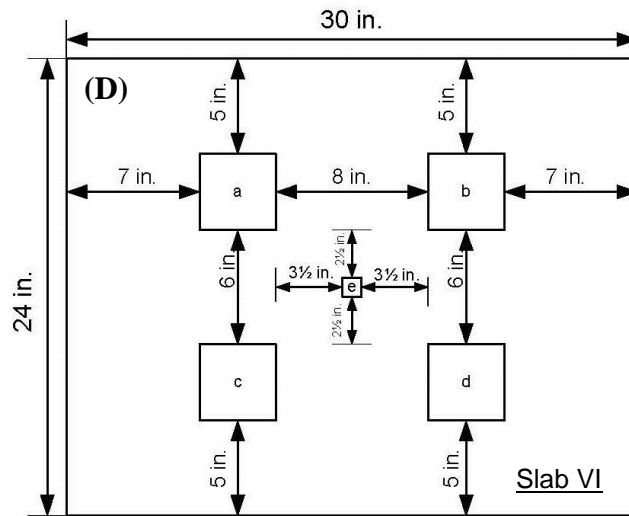
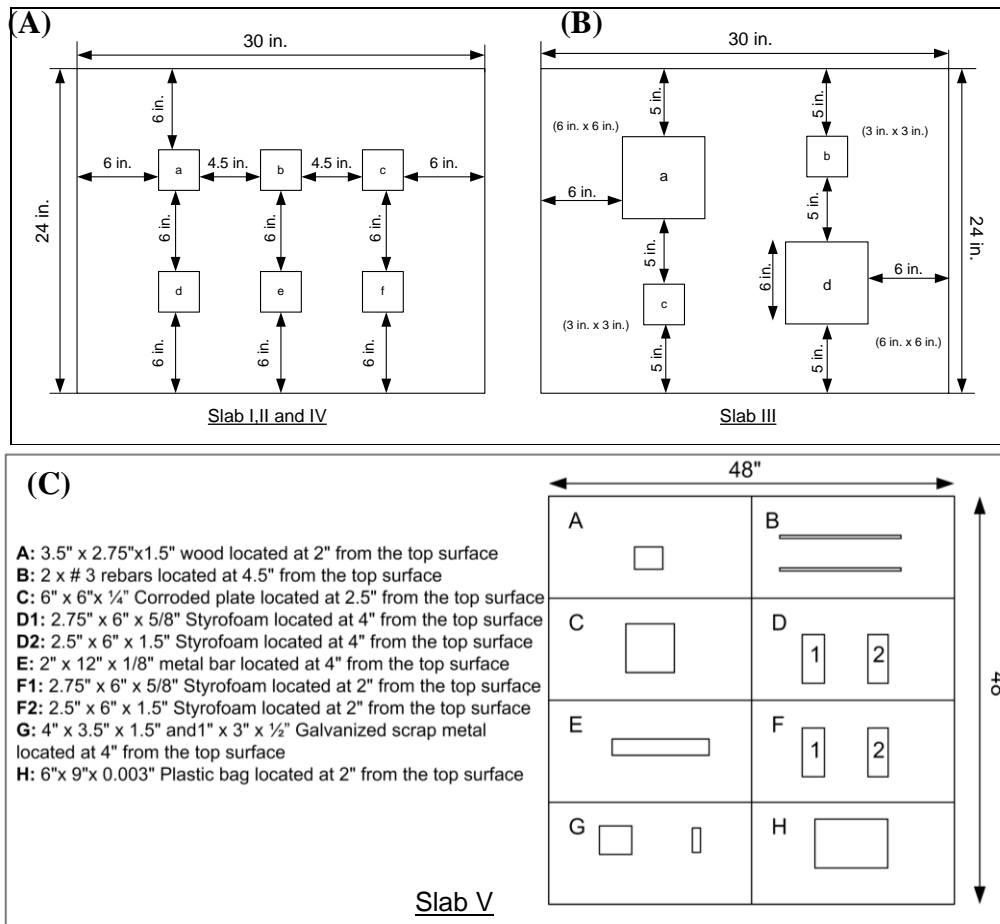
A total of six concrete slabs containing simulated delaminations were constructed for active IR thermography experiments in the laboratory, one of which was used for a parametric study to investigate several testing variables. Test Slabs I-V include a repurposed slab with dimension of 45 in. x 45 in. x 5.5 in. constructed in April 2010 (Slab V) and four 2.5 ft x 2 ft x 5.5 in. slabs that were built between November 2012 and June 2013 (Slabs I- IV). The specimen size for slabs I-IV was selected based on the field of view of the thermal infrared camera used during testing which has the capability to capture a majority of the specimen at a relatively close range (6 ft.). Specific concrete information used for constructing test slabs I-VI is summarized in Table 6-1. Because Slab V was repurposed from previous laboratory tests conducted at Michigan Technological University that were not concerned with mix design or properties, mix proportions for this test slab are unknown.

Table 6-1: Concrete Mix Design and Wet Properties for Test Slabs I-V.

<i>Properties</i>	<i>Slab I</i>	<i>Slab II</i>	<i>Slab III</i>	<i>Slab IV</i>	<i>Slab V*</i>	<i>Slab VI</i>
Cement (lb/cy)	737.5	737.5	737.5	567	-	565.8
Water (lb/cy)	312.8	312.8	312.8	270	-	216.5
Coarse Aggregate (lb/cy)	1794.4	1794.4	1794.4	1869.75	-	1865.3
Fine Aggregate (lb/cy)	765	765	765	1269	-	1366.3
Air Entrainment (oz/cy)	14.75	7.5	9.8	0	-	3.47
Slump (in.)	8.5	0	2.5	0.5	2.75	8.75
Air (%)	8.1	2.4	3.3	1.6	5	8
Date of Construction	11/15/2012	04/30/2013	05/16/2013	06/06/2013	April 2010	9/13/2013

Concrete delivered via Ready mix truck based on Michigan Department of Transportation (MDOT) grade D mix (MDOT 2003).

The plan layout for Slabs I-VI are shown in Figure 6-1. All simulated delaminations shown in Figure 6-1 (A) are 3 in. x 3 in. x 3/8 in. Styrofoam blocks. The selected defect size allowed for the placement of six delaminations in the concrete slab with sufficient distance to the edges of the specimen. Simulated delaminations in Slabs I-IV were placed at varying depths inside the concrete slabs. The Styrofoam was positioned at these various depths using fishing line and concrete was cast around the blocks. Care was taken when placing concrete to ensure the simulated delaminations remained level to the surface of the specimen and at the planned height.



(a, b, c, d) 4 in. x 4 in. x 3/8 in. Styrofoam
 (e) 1 in. x 1 in. x 3/8 in. Styrofoam

Figure 6-1: Plan Layout of Simulated Delaminations for (A) Test Slabs I, II, and IV (B) Test Slab III (C) Test Slab V and (D) Test Slab VI.

Test specimen III was constructed using Styrofoam blocks of different sizes. Simulated delaminations (a) and (d) in the plan layout for Slab III (Figure 6-1 (B)) have dimensions of 6 in. x 6 in. x 3/8 in. while delaminations (b) and (c) have dimension of 3 in. x 3 in. x 3/8 in. These sizes were selected to investigate the effects of delamination size and depth on defect detection using active IR thermography.

Slab V (shown in Figure 6-1 (C)) has larger dimensions than other test slabs. Simulated delaminations of different materials were placed in this slab for previously conducted passive infrared thermography studies (Vaghefi et al. 2011). In the current study, delaminations F1 and F2, composed of Styrofoam, were considered for investigation using active IR thermography. The impact of several test parameters including heat impulse duration, heater distance, and heater element type on the thermal contrast between delaminations and sound concrete in thermal images were investigated using Test Slab VI. This test slab is 24 in. by 30 in. by 5.5 in. and contains four 4 in. x 4 in. x 3/8 in. Styrofoam blocks and one 1 in. x 1 in. x 3/8 in. block. The blocks were positioned in the specimens using the same procedure as described for test slabs I-V at a depth of 1.5 in. from the concrete surface.

6.2.2 FLIR SC640 Thermal Imaging Camera

A FLIR ThermaCAM SC640 thermal infrared camera was used during laboratory experiments to capture temperature data on the surface of concrete specimens. This camera has a 640 x 480 pixel display with a 24° x 18° field of view and a temperature resolution of 0.1 °F. An external visual display allows for a real time image display and the alignment of test subjects. The camera was operated using ThermaCAM Researcher Professional software from a laptop computer. Several parameters, including ambient temperature, relative humidity, and emissivity, were used as inputs to the camera software prior to each test to compensate for the material properties of concrete as well as the amount of radiation reflected by the concrete surface and absorbed into the atmosphere. Images were recorded every 30 seconds to ensure that small, incremental changes in thermal contrast between delaminated areas and sound concrete were captured.

6.2.3 Heat Source

A 1500W electric Solaira infrared patio heater was selected as a viable heat source for laboratory tests based on a literature review of heat sources for active IR thermography testing on concrete elements (Vaghefi and Ahlborn 2013). Selecting a heating source is highly dependent on the thermal output desired and the depth of flaws including delaminations. In general, heat sources with a lower thermal output are effective for detecting subsurface flaws closer to the surface. Deeper defects require a higher thermal output heat source for detection. Selecting the heat source for an active IR thermography test also depends on the heating method selected for testing. Table 6-2 summarizes heating parameters and applications in previous literature.

Table 6-2: Heating Methods and Parameters for Different Applications in Civil Engineering.

<i>Heater</i>	<i>Power (W)</i>	<i>Power (Btu/hr)</i>	<i>Distance</i>	<i>Heating Duration (sec)</i>	<i>Application</i>	<i>Area</i>	<i>Source</i>
Six halogen flood lights	3200	11000	NA	NA	Voids in Concrete Slab	4 ft x 4 ft (1.2 m x 1.2 m)	(Abdel-Qader et al. 2008)
Three infrared radiator (moving along the surface)	3x2400	3x8200	6 in. (15 cm)	300, 900 , 2700	Voids in Concrete Slab	60 in. x 60 in. (1.5 m x 1.5 m)	(Maierhofer et al. 2002)
Two 250 W infrared heating lamps (200mm)	500	1710	13 in. (33 cm) 2 in. (50 mm)	10	CFRP laminates	24 in. x 9.84 in. x 1.77 in. (610 mm x 250 mm x 45 mm)	(Starnes et al. 2003)
Quartz lamp (lamine FRP)	500	1710	6 in. (152 mm)	NA	FRP laminates	3 ft ² (0.29 m ²)	(Levar and Hamilton 2003)
Kerosene heater (larger area - Fabric FRP)	22000	75000	6 in. (152 mm)	NA	FRP laminates	3 ft ² (0.29 m ²)	(Levar and Hamilton 2003)
Quartz heater	1500	5200	NA	NA	Existing RC bridge pier	NA	(Halabe et al. 2012)
Fan heater	2000	6800	NA	<300	Voids in Concrete Slab	<10.76 ft ² (<1 m ²)	(Arndt 2010)
Halogen lamp	2x650	2x2200	NA	3	FRP delaminations	6.73 ft ² (0.625 m ²)	(Arndt 2010)
Flash light	2x1500	2x5200	NA	0.10	FRP delaminations	6.73 ft ² (0.625 m ²)	(Arndt 2010)
Xenon arc lamp	6000	21000	18.7 ft (5.7 m)	950	Elevated concrete bridge FRP delamination	90.4 ft ² (8.4 m ²)	(Kurita et al. 2009)
Flash light	2 x 500	2 x 1710	7.9 in. (20 cm)	50ms	FRP composite system	72 in ² (464.5 cm ²)	(Brown and Hamilton 2007)
Scan (line heating)	2 x 500	2x 1710	3 in. (7.6 cm)	12	FRP composite system	288 in ² (1858 cm ²)	(Brown and Hamilton 2007)
Long pulse (flash lights)	2 x 500	2x 1710	7.25 in. (18 cm)	30	FRP composite system	432 in ² (2787 cm ²)	(Brown and Hamilton 2007)
Long pulse (flash lights)	2 x 500	2x 1710	7.25 in. (18 cm)	60	FRP composite system	432 in ² (2787 cm ²)	(Brown and Hamilton 2007)

NA – Information is not available in the literature.

Providing a relatively uniform heat across the concrete specimen surface and a heat impulse capable of creating visible contrast between subsurface defects and sound concrete in thermal images, the Solaira heater is compact in size, portable, and lightweight. Measuring 9 in. x 16 in. x 6 in. and weighing 7.5 lbs., this heater can be easily repositioned for testing concrete specimens in the laboratory. With the ability to heat relatively large areas of concrete at once compared to other heating techniques, this heater has the potential to be used for field applications of active IR thermography on structural concrete bridge elements.

6.2.4 Laboratory Test Set-Up and Data Collection

All laboratory testing of concrete specimens was conducted indoors at the Cement and Concrete Research Laboratory on the campus of Michigan Technological University in Houghton, Michigan. Each of the test specimens were specifically designed and constructed with simulated delaminations to investigate the feasibility of using active IR thermography to detect delaminations at different depths and sizes. The specimens were positioned horizontally on wooden shipping pallets level to the ground for testing. Before testing began, several environmental variables including the ambient temperature and humidity were measured using a handheld thermo-hygrometer, recorded for future reference, and used as input parameters to the ThermaCAM Researcher computer software used to record data throughout experiments. Because all objects absorb and emit different amounts of radiation, another important input parameter to the ThermaCAM software that accounts for material properties of concrete and allows for acquisition of accurate surface temperature data is emissivity. Emissivity describes the effectiveness of an object to emit energy as radiant temperature and can vary over the concrete surface due to the type and distribution of aggregate or the amount of moisture present from precipitation and condensation. A value of 0.95 was estimated for this material property and was considered sufficient for the purpose of detecting subsurface anomalies as the relative temperature difference between delaminations and sound concrete is most important for delamination detection and analysis methods in this study (Vaghefi 2013).

Providing a heat impulse to the surface of the concrete specimens, the infrared heater was positioned above the concrete specimens at a distance of 3.5 ft. This distance was selected to ensure that the heat impulse delivered to the test specimens was capable of producing detectable contrast between delaminations and sound concrete in thermal infrared images over a short period of time (Vaghefi 2013). The heater was positioned parallel to the concrete surface to achieve uniform heating of the test specimens and was suspended from two support arms by means of bungee cords. The support arms were clamped to two tripods positioned on either side of the slab specimens. Counter weights were used on the support arms to balance the weight of the heater over the center of the tripod.

To record changes in the surface temperature of the concrete test specimens, the FLIR was positioned at a distance of 6 ft. above the same surface of the test specimen as the heater. The camera was tripod mounted and adjusted to best capture the entire area of the specimen surface. The tripod supporting the FLIR SC640 was secured to a wood support structure constructed on

top of a wheeled cart to allow for camera repositioning. A camera angle of approximately 20° to 30° from vertical was used to ensure the image of the heater was not captured. This relatively small angle was necessary to analyze the relative shapes, locations, and depths of the simulated delaminations. Figure 6-2 shows the laboratory experimental set-up.

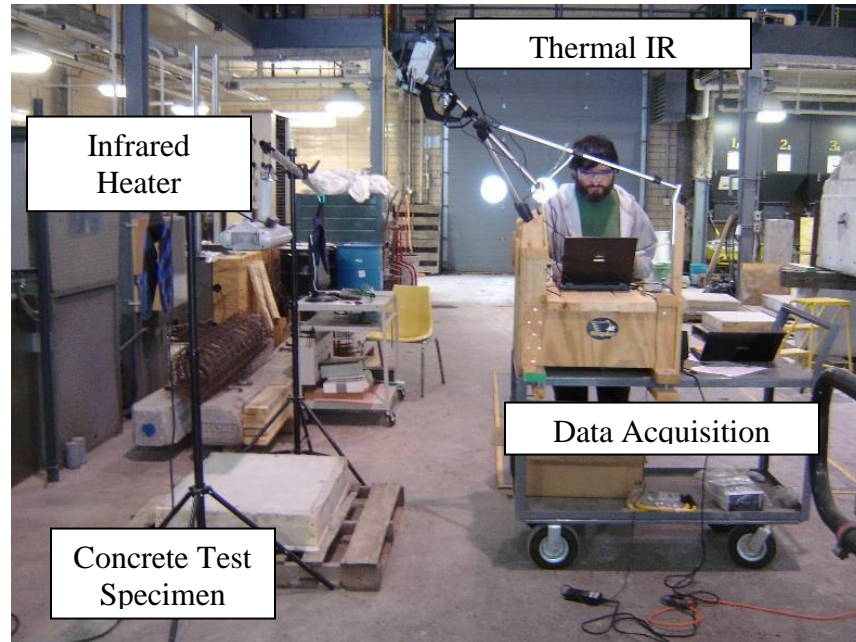


Figure 6-2: Experimental Laboratory Set-Up.

For each experimental test, data collection began immediately as the heater was turned on. After the heating period, the heater was turned off and remained in position over the specimen surface. Data collection continued for an additional period of time to ensure a majority of the heat impulse had dissipated throughout the concrete specimen and little to no thermal contrast between simulated delaminations and sound concrete could be seen in the external display of the FLIR SC640 thermal camera.

6.2.5 Thermal Imaging Analysis

Upon completion of laboratory experiments, thermal images from the test specimens were compiled and analyzed. Based on the visible temperature contrast between subsurface defects and surrounding areas of sound concrete in thermal images throughout the temporal sequence, the simulated delaminations were subjectively located. The following sections describe the analysis process to predict the depth of delaminations using estimated observation times from absolute contrast graphs.

6.2.5.1 Absolute Contrast

The absolute contrast of a defected area at a particular time ($\Delta T(t)$) is defined as the relative temperature change between the surface temperature above a suspected defected area ($T_{\text{def}}(t)$) and the surface temperature of a reference background area ($T_s(t)$) on a thermal IR image (Maldague 2001).

$$\Delta T(t) = T_{\text{def}}(t) - T_s(t) \quad \text{Equation 6-1}$$

Two different methods can be used to calculate the absolute contrast in a single infrared image: (1) consider the surface temperature difference of a single pixel above the suspected delamination and a single pixel above the background area or (2) consider the average surface temperature within the boundaries of an area above the suspected defect and above a selected background reference area close to the suspected defect (Vaghefi 2013). The second method has been proven to be more effective as it diminishes the variability in selecting only one point in the background (Brown and Hamilton 2007). Therefore, the average temperatures within the suspected defective area and the reference background area were considered for monitoring the absolute contrast of areas of delaminations (Vaghefi 2013).

The representative area above a simulated defect was selected throughout all laboratory experiments using subjective interpretation based on the size and shape of the simulated delaminations and on the visible areas of temperature contrast between suspected delamination and areas of sound concrete in the thermal infrared images (Vaghefi and Ahlborn 2013). It should be noted that the intention of the bounded area above the defect is to calculate absolute contrast with respect to the reference background area and is not necessarily an accurate representation of the actual size of the subsurface defect. The background reference area for each individual delamination can also be located subjectively, however, for this study, the reference area was defined as a rectangular box-shape around each delaminated area with a thickness of 5 pixels. This shape was chosen to account for non-uniform heating patterns across the concrete surface. Once the delaminated area and background reference area were selected, Equation 1 was used to construct an absolute contrast graph. Figure 6-3 shows the background reference area configuration on a thermal infrared image taken 6.5 minutes after the heater was turned off during one of the laboratory tests. The figure was produced in Matlab using data obtained from the ThermaCAM software. “Ref” indicates the background reference area (sound concrete) close to the delamination that was considered for determining the temperature of the background and the absolute contrast of each delamination.

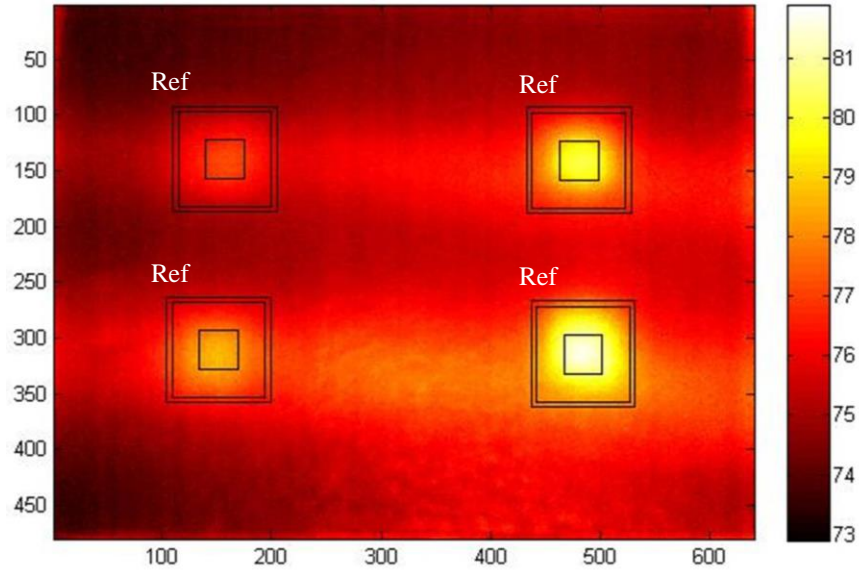


Figure 6-3: Selected Delamination Area and Background Reference Area for Slab VI used to Calculate Absolute Contrast.

Figure 6-4 shows the absolute contrast variation of delaminations for one of the laboratory experiments using a reference background. Absolute contrast graphs are obtained to determine the observation time of each simulated delamination and to estimate the depth of delaminations relative to one another based on the values of maximum absolute contrast. For example, from the graphs presented in Figure 6-4, it can be seen that delaminations (c) and (f) appeared with higher absolute contrast values than delaminations (a) and (d) and can therefore be estimated as deeper defects.

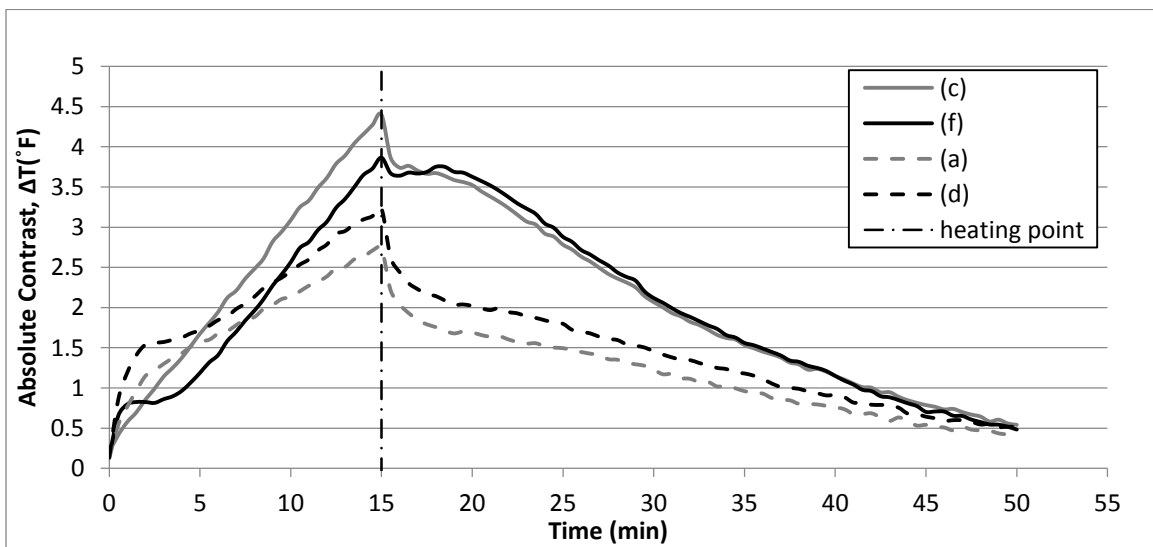


Figure 6-4: Absolute Contrast Variation above Simulated Delaminations for one of the Conducted Laboratory Tests.

6.2.5.2 Observation Time

Observation time is defined as the time at which delaminated areas appear on a thermal infrared image with the maximum absolute contrast after the heating period of active IR thermography or at the vertex of negative convexity of the absolute contrast variation graphs (Vaghefi 2013). Observation time is determined by monitoring the absolute contrast of each suspected delamination during both the heating and cooling periods of active IR testing. Because observation time is dependent on the interpretation of the absolute contrast graphs, the method of calculating absolute contrast and the subjective selection of defect areas and sound concrete background reference areas will have an effect on estimating this time step value (Vaghefi 2013). Figure 6-5 shows a diagram depicting the process of determining the observation time using an absolute contrast graph.

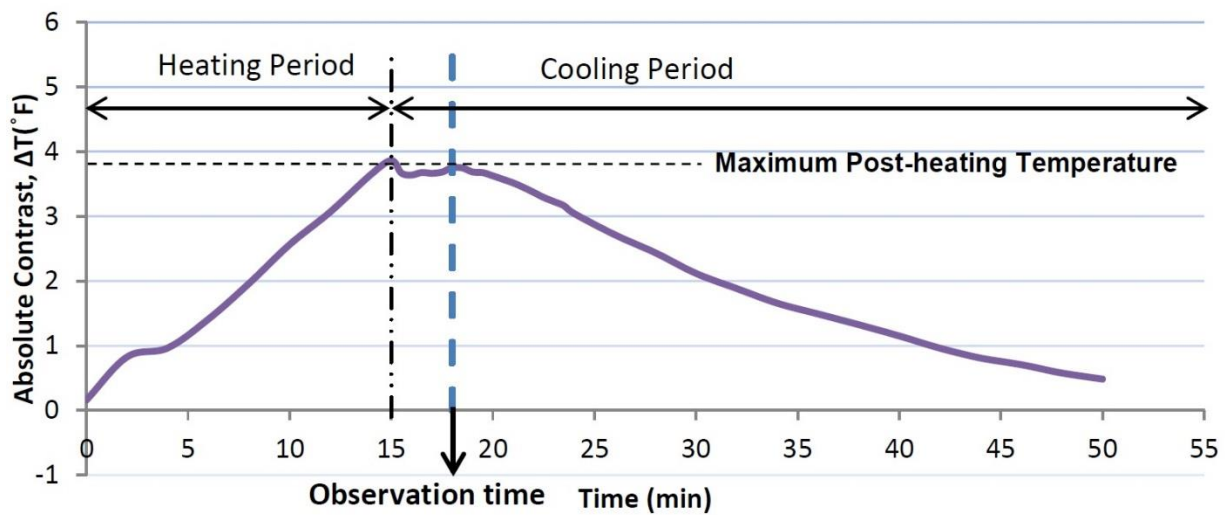


Figure 6-5: Definition of Observation Time Shown on an Absolute Contrast versus Time Graph Obtained from an Active IR Thermography Test.

6.2.5.3 Delamination Depth Computation

The theory of active IR thermography testing suggests that the depth of flaws and delaminations can be estimated using results obtained from monitoring the temperature change on the test specimen surface and determining the observation time of each delaminated layer (Maldague 1993). In general, during infrared thermography testing, deeper delaminations appear on the thermal infrared images with less contrast to surrounding sound concrete than shallower delaminations. The relationship between observation time and depth is shown in Equation 6-2 and was proven previously to be valid for estimating the depth of the delaminations in concrete slabs (Vaghefi 2013).

$$t \approx \frac{z^2}{8} \quad \text{Equation 6-2}$$

where, t is the observation time, z is the defect depth, and δ is thermal diffusivity of the material as defined by Equation 6-3.

$$\delta = \frac{K}{\rho C} \quad \text{Equation 6-3}$$

where K is thermal conductivity, ρ is material density and C is thermal capacity or material specific heat (Maldague 1993; Ghosh and Karbhari 2006). Thermal diffusivity of concrete depends on the type of the coarse aggregate used in concrete. The general range of thermal diffusivity of concrete is between 0.016 ft²/h (for expanded shale aggregate) and 0.085 ft²/h (for quartz aggregate) (Lamond and Pielert 2006).

6.2.5.4 Relationship between the observation time and the depth of delamination

According to Equation 2, observation time (t) has a quadratic relationship with the depth of the defect (z). To discuss and prove the relationship between the observation time and the depth of the defect, the observation time for each delamination was plotted against the square of the delamination depth obtained from ground truth information. A linear regression line was then drawn to obtain the accuracy of the relationship between t and z^2 and estimate the thermal diffusivity for the concrete laboratory test specimens.

6.3 Results of Laboratory Experiments

Laboratory experiments were conducted for this study to prove the concept of active IR thermography applied to concrete specimens prior to field applications of this non-destructive remote sensing technology. Thermal contrast between subsurface anomalies and sound concrete in thermal images was used to investigate the accuracy of Equation 2 for test slabs I-V. The relationship between delamination size and depth to absolute contrast was also investigated for these test slabs. In addition, a parametric study was conducted on test specimen VI to investigate the effects of the heat impulse duration, heater distance, and heater element type on the thermal contrast between delaminations and sound concrete in thermal images. The concrete test specimens and results from each laboratory experiment are described in the following sections. For a more in-depth discussion regarding delamination depth estimation using absolute contrast please reference Khatera Vaghefi's dissertation work (Vaghefi 2013).

6.3.1 Delamination Depth and Delamination Width to Depth Ratio

Laboratory tests conducted on concrete specimens I-V emphasized delamination depth analysis procedures using absolute contrast graphs constructed from thermal IR data. In addition, the ratio of the delamination depth to the delamination radius (width) was observed to determine the dimensions and depth at which delaminations are no longer detectable using the described analysis methods.

6.3.1.1 Measured Depth of Delaminations

To validate the testing results and obtain the relationship between the depth of delaminations and observation times, 4 in. diameter cores were extracted at the locations of simulated delaminations upon completion of active IR thermography testing on concrete Slabs I-V. A summary of the measured depths of the Styrofoam blocks and the width-to-depth ratios for each simulated delamination in test slabs I-V are provided in Table 6-2. Depth of the Styrofoam block was measured from the top surface of the core (concrete slab) to the top surface of the Styrofoam layer using a micrometer with a 0.01 in. resolution.

Table 6-2: Measured Depth of Simulated Delaminations and Width-to-Depth Ratio Obtained from the Extracted Cores of Test Slabs I-V.

<i>Core No.</i>	<i>Measured Depth Determined by coring (in.)</i>	<i>Width-to-Depth Ratio</i>	<i>Core No.</i>	<i>Measured Depth Determined by coring (in.)</i>	<i>Width-to-Depth Ratio</i>
Slab I-a	1.04 *	2.89 **	Slab III-a	1.92*	3.12**
Slab I-b	2.20	1.36	Slab III-b	2.96	1.01
Slab I-c	0.72 *	4.16**	Slab III-c	1.37*	2.19**
Slab I-d	1.14*	2.64**	Slab III-d	3.18	1.89
Slab I-e	2.13	1.41	Slab IV-a	1.81*	1.66
Slab I-f	0.75*	3.98**	Slab IV-b	1.03*	2.91**
Slab II-a	2.72	1.10	Slab IV-c	1.46*	2.06**
Slab II-b	3.34	0.90	Slab IV-d	2.36	1.27
Slab II-c	2.95	1.02	Slab IV-e	2.15	1.39
Slab II-d	1.27*	2.36**	Slab IV-f	1.92*	1.57
Slab II-e	2.37	1.27	Slab V-F2	0.33*	7.66**
Slab II-f	2.43	1.24	Slab V-F1	0.89*	3.10**

*depth (z) < 2 in.

** width/depth (R) > 2

6.3.1.2 Data Collection and Procedure

Thermal infrared images were collected from test Slabs I-V using the surface heating method during a 50 minute test period which included a 15 minute heat time and a 35 minute cooling period. Table 6-3 summarizes the environmental conditions that were used as inputs in the ThermaCAM computer software for data collection.

Table 6-3: Environmental Conditions for Active IR Testing on Concrete Slabs I-V.

<i>Test Specimen</i>	<i>Humidity (%)</i>	<i>Ambient Temperature (°F)</i>
Slab I	14.1%	72.3°F
Slab II	37%	73°F
Slab III	32%	75°F
Slab IV	51%	76.2°F
Slab V	19.2%	67.8°F

6.3.1.3 Results and Analysis

Upon completion of active IR thermography testing on test slabs I-V, areas of suspected delamination and background reference areas were identified. Figure 6-6 shows the selected delamination areas and background reference areas for test slabs V and III. The dimensions, given in pixels, of the selected areas are also shown on the figure.

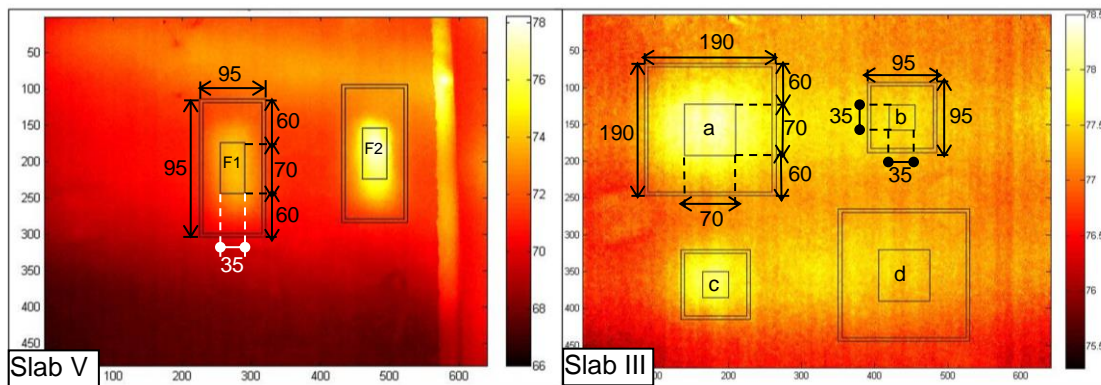


Figure 6-6: Boundaries Selected for Areas of Delamination and the Associated Background Reference Areas for Concrete Test Slabs V and III.

Average temperature within the selected areas was monitored over both the heating and cooling periods at 30 second intervals, and absolute contrast between the suspected delaminated area and reference background was determined and plotted. Figure 6-7 shows the absolute contrast of delaminated areas that were apparent on thermal infrared images collected from each slab. The depth of the delamination presented on the plots indicates the measured depth of the delaminations obtained by coring. From the absolute contrast graphs in Figure 6-7, observation time was estimated for the eleven simulated delaminations that were apparent in the recorded thermal images. The estimated observation times are presented in Table 6-4.

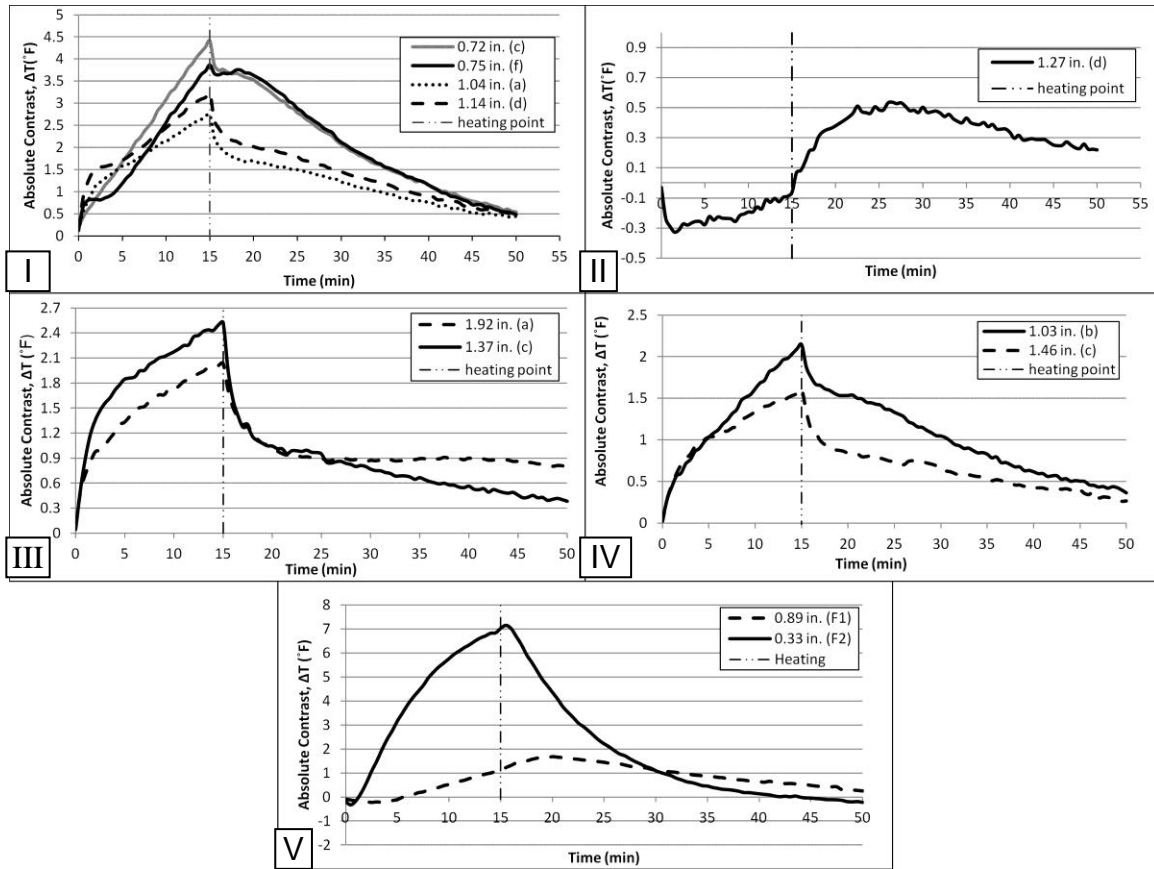


Figure 6-7: Absolute Contrast Variation above each Simulated Delamination during Active IR Thermography Testing on Test Slabs I-V.

Table 6-4: Observation Time and Corresponding Absolute Contrast for each Suspected Area of Delamination, Obtained from the Absolute Contrast Variation Plots.

<i>Delamination No. (Depth)</i>	<i>Observation time (min)</i>	<i>Corresponding Absolute Contrast (°F)</i>
I-a (1.04 in)	4.5	1.7
I-c (0.72 in)	1.0	3.74
I-d (1.14 in.)	6.5	2.03
I-f (0.75 in.)	3.0	3.75
II-d (1.27 in.)	7.5	0.51
III-a (1.92 in.)	12.5	0.89
III-c (1.37 in.)	8.5	0.99
IV-b (1.03 in.)	5.5	1.54
IV-c (1.46 in.)	12.0	0.75
V-F2 (0.33 in.)	0.5	7.16
V-F1 (0.89 in.)	5.0	1.68

6.3.1.4 Discussion

To develop the relationship between the depth and the observation time of each simulated delamination, observation time for each simulated delamination was plotted against the square of the measured depth. The linear regression line was drawn to confirm the linear relationship between t and z^2 and the square of the correlation coefficient (R^2) was determined to be 0.896 (Figure 6-8).

Although, different mixes were used for the construction of the five slabs, the aggregate type for all these slabs were similar and were according to the Michigan Department of Transportation (MDOT) Standard Specification for Construction (MDOT 2003). Thus, an approximate value for the thermal diffusivity was estimated based on the results of the active IR thermography test on the concrete test slabs. From the linear regression equation, thermal diffusivity can be estimated as 0.2219 in²/min (0.092 ft²/h), which is approximately the thermal diffusivity for concrete containing quartz aggregate (0.085 ft²/h).

The linear regression equation obtained from the data set presented in Figure 6-8 proves that observation time is a function of the square of the depth in the first approximation. Thus, the relationship defined in Equation 2 is a valid relationship for concrete material, and the depth of delaminations can be estimated based on the observation time of each delaminated area. One unexpected variable within the presented experiment was the air content of each test slab which is reported in Table 6-1 and again in Figure 6-8. Further investigations were conducted regarding the effect of concrete air content on delamination observation time which are beyond the scope of this study. For more information about concrete air content considerations for determining observation time, please reference Khatereh Vaghefi's thesis work entitled "Infrared Thermography Enhancements for Concrete Bridge Evaluation" (Vaghefi 2013).

From the results of the active IR thermography testing, it can be seen that the observation time for delaminations appeared between 0 and 12.5 minutes after the heat source was turned off. This observed time period can help in identifying the time at which thermal infrared images should be captured to obtain the vertex of negative convexity on the thermal infrared images, specifically in situations where location and size of the delamination are of interest rather than the depth of the delamination. Note that the time period determined from the results of this study is specific to the heat source and the selected distance between the concrete slab surface and the heat source (3.5 ft). Additional studies must be conducted to generalized the relationship between the observation time period, heater, heater distance, and diffusivity of the concrete.

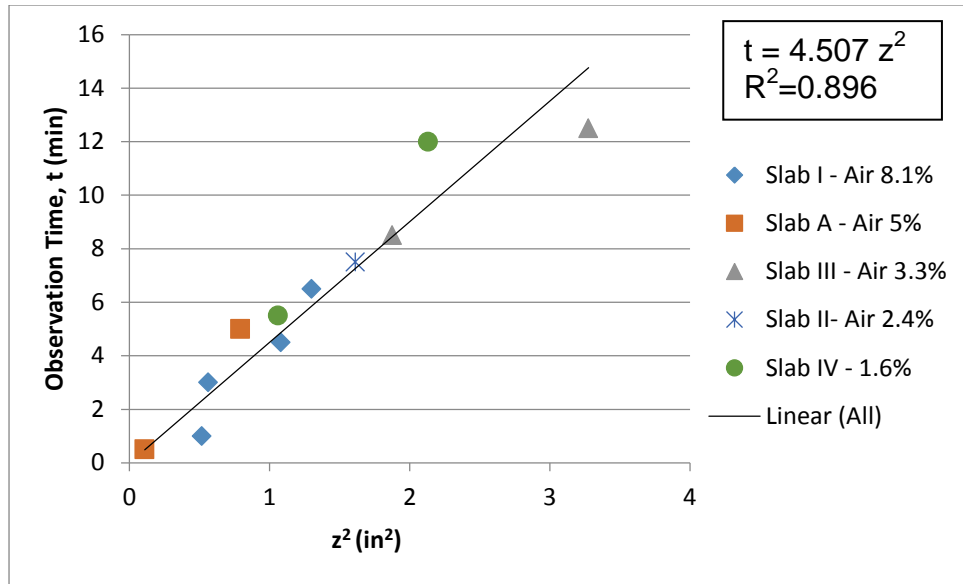


Figure 6-8: Observation Time Versus the Square of the Depth of each Detected in Active IR Thermography Testing of Test Slabs I-V.

Another important observation from the results of active IR thermography testing on concrete slabs I-V is that only delaminations with a depth less than or equal to 2 in. and with a width-to-depth ratio greater than 2 were detected using the current test method, equipment and analysis method. Delaminations with a depth of less than 2 in. are shown with one asterisk in Table 6-2 and delaminations with a width-to-depth ratio (R) value greater than 2 are shown with two asterisks. Results show that delaminations can only be detected when both limits are satisfied. For example, delamination “a” in Slab IV was located 1.81 in. from the top concrete surface but had a width to depth ratio of less than 2, thus it was not detected during the active IR thermography testing. The effects of delamination size and width-to-depth ratio on detecting subsurface defects in concrete is in agreement with the previously discussed empirical rule for infrared thermography (Maldague 1993). Further investigations regarding heater output and distance from the concrete specimen of interest should be conducted to determine the possibility of detecting delaminations at greater depths.

6.3.1.5 Conclusions

Results from laboratory testing on concrete test Slabs I-V provide evidence to verify the capabilities of pulsed (active) infrared thermography to predict the location and estimate the depth of delaminations in concrete bridge elements. Data confirms the linear relationship between the square of the depth and observation time for subsurface defects suggesting that the observation time is generally between 0 and 5 minutes for delaminations with a depth less than 1 in. and between 5 and 20 minutes for delaminations with a depth between 1 and 2 in. In addition, results from active IR thermography testing contribute additional evidence supporting the capabilities of this remote sensing technology to detect delaminations shallower than 2 in. deep and with a width-to-depth ratio greater than 2. Further study is required to investigate the

maximum depth and the minimum width-to-depth ratio at which delaminations can be detected using active IR thermography. The methodology of estimating depth from the results of an active IR test on concrete specimens and the discussion about the effects of the width-to-depth ratio in detecting delamination has introduced a method of infrared thermography data interpretation that serves as a base for future studies.

The laboratory study conducted on test specimens I-V was limited by the specific distances between the camera, the test specimen and the heat source. Heating sources with higher heating output and various distances between the heat source and the concrete test specimens should be further investigated to identify the most suitable heat source for field applications, and the practical distance between the heat source and concrete surface for accurate delamination detection.

Recognizing that all laboratory tests were conducted indoors, one of the major concerns for applying active IR thermography in the field is the possible conflicts between ambient temperature change caused by heating effects of the sun and the use of an external heating source to create the necessary temperature gradient for active IR thermography testing. Depth prediction and size determination of subsurface defects should be further investigated while exploring the influence of environmental conditions.

6.3.2 Parametric Study 1: Heat Impulse Duration

The objective of parametric study 1 conducted on concrete specimen VI was to investigate the effects of shortening the thermal impulse duration on the thermal contrast of simulated delaminations and determine the feasibility of shorter inspection times on the bridge deck underside and fascia beams. Heat times of 5 minutes and 10 minutes were investigated and compared to the results of a control test using a 15 minute heat time. All other testing variables remained constant throughout the experiment. However, for the purpose of improving equipment positioning capabilities, reducing experimental set-up time and the ease of equipment transport for future field applications, two mounting systems were custom fabricated for the FLIR SC640 thermal camera and infrared heater. The mounting systems were constructed using aluminum square tubing and were supported by collapsible tripods. Counter weights were used to balance the weight of the test equipment. The new mounting systems allowed for greater versatility in positioning the equipment for testing concrete elements in different orientations.

Two laboratory tests were conducted on concrete specimen VI using the aforementioned methodology and heat impulse durations less than 15 minutes. For each test, data collection began immediately as the heater was turned on and continued for a total of 60 minutes to ensure that a majority of the heat impulse dissipated through the concrete specimen and little to no thermal contrast could be seen between delaminated areas and areas of sound concrete in thermal images. The environmental conditions measured prior to testing and included as inputs to the ThermaCAM computer software are summarized in Table 6-5.

Table 6-5: Environmental Conditions for Active IR Testing on Concrete Slab VI for Heat Time Investigation.

<i>Heat Impulse Duration (min)</i>	<i>Humidity (%)</i>	<i>Ambient Temperature (°F)</i>
5	5.9	72.3
10	25.5	65.6
15	6.6	72.5

6.3.2.1 Results and Analysis

Areas of suspected delamination and sound concrete background reference areas were selected upon completion of active IR thermography testing on test slab VI using shortened heat times. These areas were monitored throughout the testing period and absolute contrast graphs were constructed. Results from the 5 minute and 10 minute tests were then compared to the 15 minute control test. Thermal images obtained from laboratory testing and the analysis areas selected for Delamination 4 can be seen in Figure 6-9. The absolute contrast graphs for each of the four simulated delaminations are shown in Figure 6-10 for the 5 minute, 10 minute and 15 minute tests. After construction of the absolute contrast figures, observation times were estimated for each delamination. The estimated observation times are reported in Table 6-6.

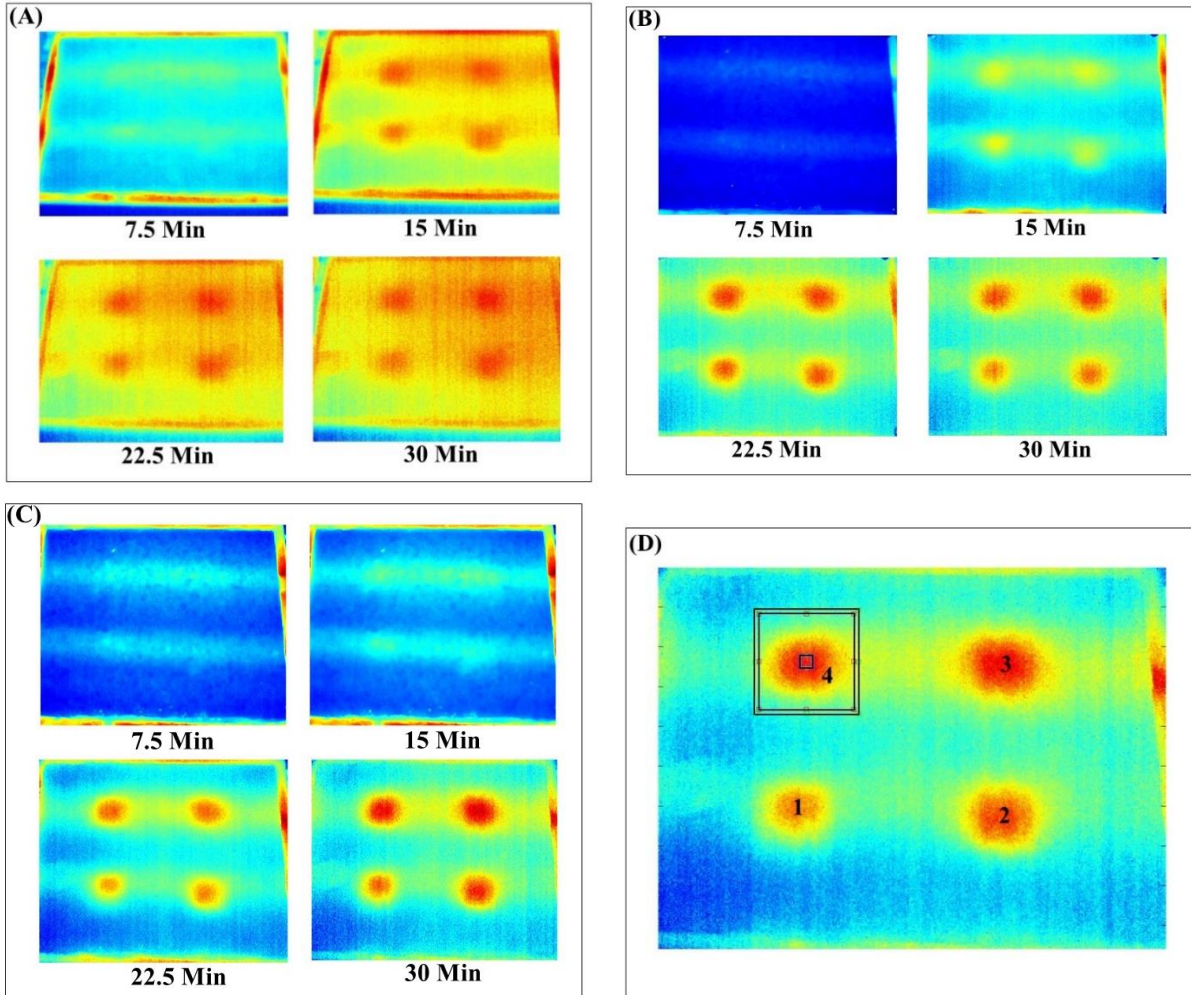


Figure 6-9: Thermal Images Captured during Parametric Experiment 1 (A) 5 Min. Heat Impulse (B) 10 Min. Heat Impulse (C) 15 Min. Heat Impulse Control Test (D) Delamination Numbering System and Selected Areas for Analysis for Delamination 4.

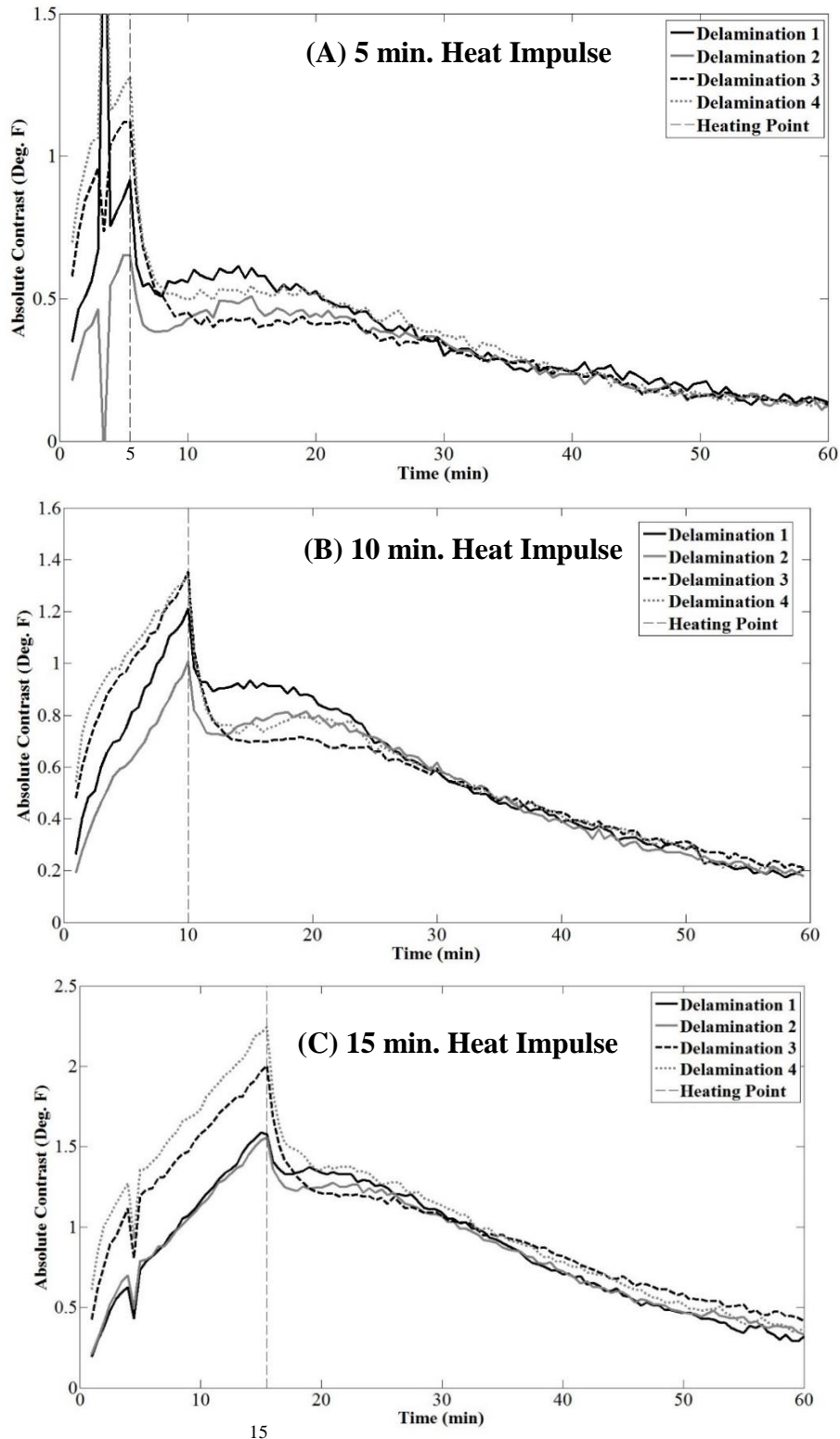


Figure 6-10: Absolute Contrast Graphs Constructed from Heat Impulse Durations of (A) 5 Minutes (B) 10 Minutes and (C) 15 Minutes

Table 6-6: Estimated Observation Times and Corresponding Absolute Contrast for Simulated Delaminations in Concrete Test Slab VI Tested with Different Heat Impulse Durations.

<i>Heat Impulse Duration (min)</i>	<i>Delamination Number</i>	<i>Observation Time (min)</i>	<i>Corresponding Absolute Contrast (°F)</i>
5	1	9.0	0.6
	2	10.0	0.5
	3	18.0	0.4
	4	19.0	0.5
10	1	10.0	0.9
	2	9.5	0.8
	3	14.5	0.7
	4	8.5	0.8
15	1	4.0	1.4
	2	7.0	1.3
	3	11.0	1.2
	4	8.5	1.3

6.3.2.2 Discussion and Conclusions

Results from active IR tests conducted on concrete specimen VI show that changing the duration of the thermal impulse directly affects the thermal contrast between areas of suspected delamination and areas of sound concrete. Decreasing the heat impulse duration from a control test of 15 minutes to 5 minutes and 10 minutes resulted in less thermal contrast between simulated delaminations and surrounding areas of intact concrete. The acquired thermal images and absolute contrast graphs also show that delaminations appear sooner in the thermal temporal sequence when exposed to shortened impulse durations than longer heat times. During active IR testing, delaminations do not become visible in thermal images until after the heating phase when the heater is turned off or removed from the vicinity of the test area. Therefore, changing the duration of the heat impulse also changes the observation time period at which delaminations appear with maximum contrast to surrounding areas of concrete.

It should be noted that the 1 in. x 1 in. simulated delamination located in the center of test slab VI did not appear in any of the active IR thermography tests conducted to investigate heat impulse duration. With a width-to-depth ratio of less than two, it was expected that this Styrofoam block would not be detected using current analysis procedures based on the findings of previous laboratory tests. Additional width-to-depth delamination studies are recommended using test slab VI, specifically with a focus on the 1 in. x 1 in. simulated delamination, for improvements in testing procedures to detect delaminations with a width-to-depth ratio less than two. It should also be noticed that thermal images collected in this experiment show a heat concentrated boarder around the test specimen. Test specimen VI was constructed using 2 x 4

wood framework which remains attached to the test slab. Due to the difference in emissivity between wood and concrete, the wood frame around this test slab appears at a different temperature in thermal images compared to concrete. These areas were avoided during the construction of absolute contrast graphs and illustrates the importance of understanding the correlation between emissivity and objects seen in thermal infrared images. For this reason, optical images are strongly recommended for field demonstrations to explain thermal anomalies.

Absolute contrast graphs in Figure 6-11 reveal absolute contrast spikes during the heating phase of the 15 minute and 5 minute tests. Although the interest of these graphs lies in the cooling phase and the distinct rise or vertex in absolute contrast to estimate observation time of delaminations, these temperature spikes must be addressed to explain experimental outlier data. The FLIR SC640 thermal camera contains an internal calibration shutter that triggers automatically to ensure accurate temperature readings based on initial calibrations from environmental conditions. As the camera captured images at a rate of two images per minute, the calibration shutter continued to trigger throughout the testing period and was captured in one of the thermal images. The shutter caused thermal distortion in the image and resulted in erroneous temperature readings. It is recommended that operators conducting active IR thermography testing in field applications be familiar with their thermal camera functions to explain unexpected variations in temperature readings.

Laboratory experiments investigating the effects of changing the thermal impulse duration on thermal contrast between areas of delamination and sound concrete areas has also led to the consideration of heater specifications and their influence on the selection of an appropriate thermal impulse duration. When selecting an impulse duration, one should consider both the power output of the heater as well as the time it takes for heater elements to reach maximum operating temperature. If a short impulse duration is selected for experimentation, the maximum power output of the heater may not contribute to the thermal contrast between delaminations and areas of sound concrete if the heater is not capable of reaching maximum operating temperature in that time period.

6.3.3 Parametric Study 2: Effect of Heating Elements on Thermal Banding

The objective of parametric study 2 conducted on concrete specimen VI was to confirm that thermal banding present in thermal images acquired from previous laboratory tests is a function of the selected heat source used for experimentation. In addition, results from this test were used to investigate the effects of thermal banding on analysis procedures used in the lab and to consider the impact of this phenomenon on analysis procedures used in the field. All testing variables described in section 6.3.2 remained constant throughout experimentation, including the 15 min. heating time, except the orientation of the infrared heater was rotated 90° compared to the heater position of previous laboratory tests. Data collection began immediately as the heater was turned on and continued for a total of 30 minutes. The environmental conditions measured prior to testing and included as inputs to the ThermoCAM computer software are summarized in Table 6-7.

Table 6-7: Environmental Conditions for Active IR Testing on Concrete Slab VI for Thermal Banding Investigation.

<i>Heat Orientation</i>	<i>Humidity (%)</i>	<i>Ambient Temperature (°F)</i>
Original Position	5.9	72.3
Rotate 90°	24.6	66.9

6.3.3.1 Analysis and Results

To determine the effects of rotating the heater on thermal concentrations and banding on the specimen surface, visual analysis procedures were used upon completion of active IR thermography testing on concrete test Slab VI. Results were compared to the 15 min. heat time control test with the heater in its original test set-up position. Four thermal images captured from both the control test and rotated heater test are shown in Figure 6-11.

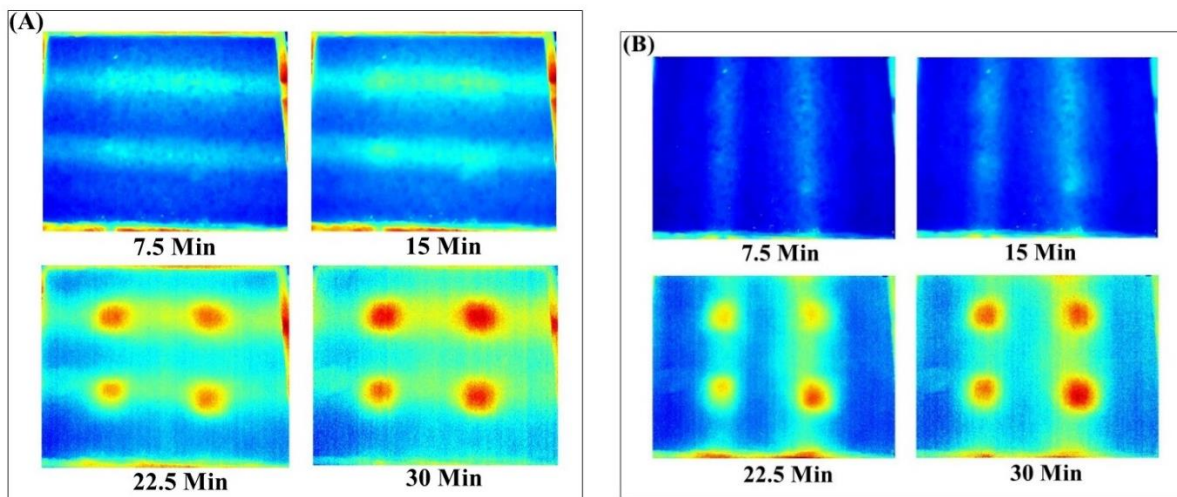


Figure 6-11: Thermal Images Captured during Parametric Study 2 (A) Control Test with Original Heater Position (B) Test with Rotated Heater Position.

6.3.3.2 Discussion and Conclusions

Rotating the infrared heat source 90° and conducting an active IR test on concrete specimen VI confirms that thermal banding shown in thermal images is a function of the heater. The Solaira infrared patio heater used to deliver the heat impulse for laboratory experiments contains a single tube element and a curved reflective heater backing. The angled construction of the heater backing causes a concentration of infrared energy on either side of the heating element and results in two distinct thermal bands on the concrete surface after the heating period. Depending on the orientation of the heater, thermal bands appear differently in successive tests. Due to this

non-uniform heating phenomenon and the subjectivity of selecting representative areas of delamination and areas of sound concrete for analysis procedures, thermal banding has a direct impact on the absolute contrast between delaminations and sound concrete. However, delaminations are still identifiable.

A more uniform heating of the concrete surface may be achieved by using a different heat source. Heaters with multiple heating elements may provide a more distributed thermal impulse making areas of delamination and areas of sound concrete more distinguishable from each other in thermal images. In addition, increasing the distance of the heater from the concrete surface may decrease the effects of thermal banding and provide a more uniformly heated area. However, increasing the heater distance will likely decrease the absolute contrast between areas of delamination and areas of sound concrete for the same heating duration. Further investigations regarding the effects of heater distance on thermal banding and absolute contrast are recommended before field applications of active IR thermography using the presented test method. It should also be noted that heaters of different types will have different heating effects on the surface of the test area. It is especially important for operators conducting active IR thermography tests to understand the heating behavior of their specific heater and how it will effect analysis procedures.

6.3.4 Parametric Study 3: Heater Distance

The objective of parametric experiment 3 conducted on concrete specimen VI was to determine the effects of changing the distance between the infrared heat source and concrete specimen on the thermal contrast between areas of delamination and sound concrete to select an appropriate distance for field applications. A distance of 2 ft. between the infrared heater and concrete specimen surface was chosen and results were compared to a control test using a distance of 3.5 ft. All other testing variables remained constant as previously discussed in the test set-up section 6.3.2, including the 15 min. heating time. Data collection began immediately as the heater was turned on and continued for a total of 60 minutes to ensure that a majority of the heat impulse dissipated through the concrete specimen and little to no thermal contrast could be seen between delaminated areas and areas of sound concrete in thermal images. The environmental conditions measured prior to testing and included as inputs to the ThermoCAM computer software are summarized in Table 6-8.

Table 6-8: Environmental Conditions for Active IR Testing on Concrete Slab VI for Heat Distance Investigation.

<i>Heat Distance from Specimen Surface (ft)</i>	<i>Humidity (%)</i>	<i>Ambient Temperature (°F)</i>
3.5	5.9	72.3
2	11.8	71.7

6.3.4.1 Analysis and Results

Upon completion of active IR thermography testing, areas of suspected delamination and sound concrete background reference areas were selected. These areas were monitored throughout the testing period and absolute contrast graphs were constructed. Results from the test were then compared to the control test with the heater positioned 3.5 ft. from the concrete surface. Thermal images obtained from laboratory testing and the representative areas selected for analysis are shown in Figure 6-12 and Figure 6-13 respectively. The absolute contrast graphs for each simulated delamination in concrete slab VI are shown in Figure 6-14 for the heater positioned 3.5 ft. and 2 ft from the specimen surface. After construction of the absolute contrast figures, observation times were estimated for each delamination and are reported in Table 6-9.

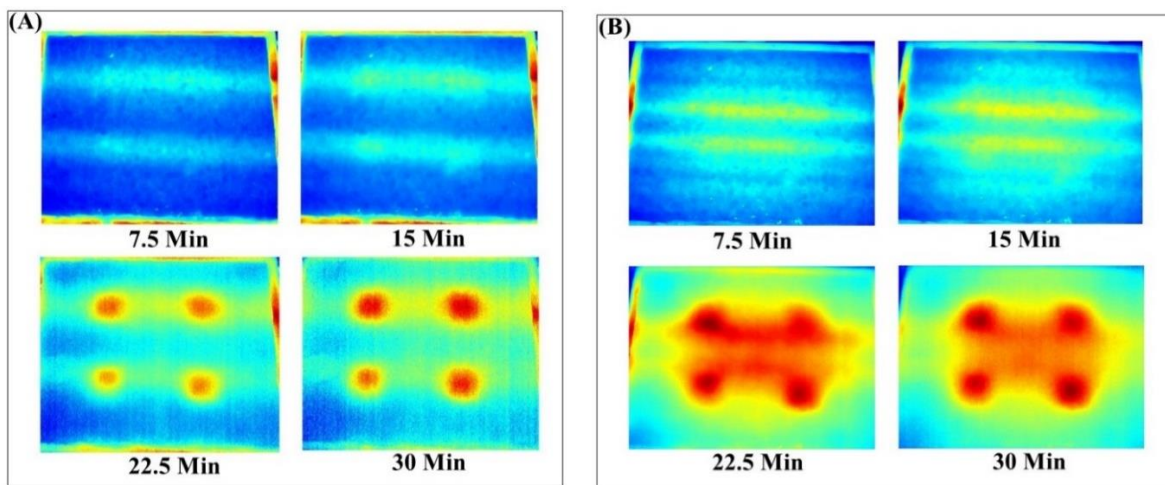


Figure 6-12: Thermal Images Captured During Parametric Experiment 3 (A) Control Test with Heater Placed 3.5 ft. from Test Specimen Surface (B) Heater Placed 2 ft. from Test Specimen Surface.

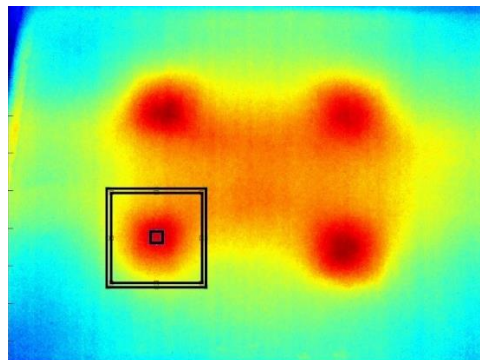


Figure 6-13: Selected Area of Suspected Delamination and Sound Concrete Area for the Active IR Test Conducted on Test Slab VI Using a 2 ft. Heater Distance from the Specimen Surface.

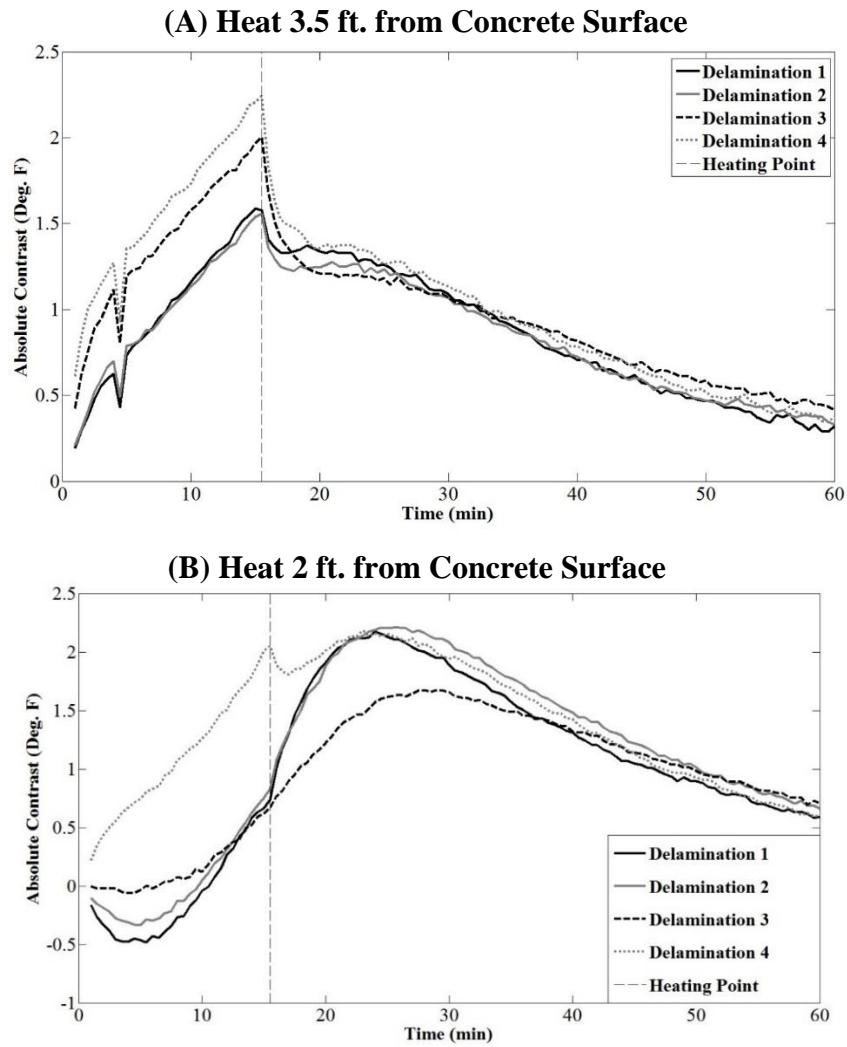


Figure 6-14: Absolute contrast graphs constructed from heater distances of (A) 3.5 ft and (B) 2 ft.

Table 6-9: Estimated Observation Times and Corresponding Absolute Contrast for Simulated Delaminations in Concrete Test Slab VI Tested with Different Heater Distances.

<i>Heater Distance from Specimen Surface (ft)</i>	<i>Delamination Number</i>	<i>Observation Time (min)</i>	<i>Corresponding Absolute Contrast (°F)</i>
3.5	1	9.0	0.6
	2	10.0	0.5
	3	18.0	0.4
	4	19.0	0.5
2	1	9.0	2.2
	2	9.5	2.2
	3	14.0	1.7
	4	8.0	2.2

6.3.4.2 Discussion and Conclusions

Results from the laboratory test conducted on concrete specimen VI suggest that changing the distance between the heat source and the surface of the concrete specimen changes the uniformity of heating. Thermal banding originating from the heater's reflective backing is more prominent during the heating phase of testing for the test conducted with the heater positioned 2 ft. from the specimen surface than the control test with the heater positioned above the specimen surface at 3.5 ft. Thermal images also show a heat concentration in the middle of concrete specimen VI directly below the infrared heater for the 2 ft. test but not in the control test (Figure 6-13). This heat concentration resulted in higher surface temperatures above the center of the test slab compared to previous laboratory tests and may make detecting delaminations by visual inspection more challenging. With the basic understanding of heat transfer and the fact that relative depths of delaminations can be estimated directly from thermal images based on thermal contrast to areas of sound concrete, the subjective analysis procedures used to locate delaminations in this study may lead to false positive results. For example, sound concrete appearing at higher temperatures due to heat concentrations may be misidentified as delaminations.

In addition to the challenges presented to visual delamination detection from non-uniform heating, heat concentrations are also shown to have a direct impact on the absolute contrast of delaminations. From Figure 6-14 it can be concluded that observation time is more easily defined from the results of the test conducted with the heater positioned at 2 ft from the specimen surface. Although this may be the case for the selected analysis areas as shown in Figure 6-14, it may not be true in all testing cases. As previously mentioned, one of the main challenges in active IR thermography analysis is selecting appropriate areas representing delaminated areas and sound concrete areas. These areas ultimately define the absolute contrast graph and observation time. Due to the bias of this experiment and knowing the locations of the simulated delaminations, heat concentrations were not misidentified as areas of delamination and were included in the background reference area. The resulting absolute contrast graph shown in Figure 6-14 will differ from a graph constructed with a background reference area not including areas of concentrated heat.

Furthermore, the results of this test provide insight on selecting an appropriate heater distance for active IR thermography testing. For the Solaira infrared heater used in this study, it can be advised that a heating distance greater than two feet from the surface of the concrete specimen should be used to ensure uniform heating and prevent thermal concentrations and banding. Further investigations are recommended to explore the relationship between heater distance and the duration of the heat impulse to ensure significant thermal contrast between areas of delamination and areas of sound concrete for the estimation of observation time.

6.4 Active IR Field Application Spring 2014

Using the test set-up and methodology developed through the laboratory testing, active IR thermography was applied to an in-service concrete bridge for condition assessment. One objective of the field application included the confirmation of active IR thermography capabilities to detect delaminations on the bridge deck underside not exposed to passive solar heating and fascia beams. Another objective was to determine the influence of heating times (5 min. versus 15 min.) in the field. In addition, the capability of using this non-destructive, remote sensing technique to estimate subsurface defect depth was also investigated.

6.4.1 Demonstration Site

MDOT structure No. 4947 – Franklin Street over US-131 and CSX railroad line is located in Kent County in Grand Rapids, Michigan. The structure spans both the north and south bound US-131 traffic lanes as well as the north and south bound CSX railroad lines. This site was selected for the application of active IR thermography due to the accessibility to the underside to the bridge. Open land access to the underside of the bridge on the east side of the structure allowed testing to be conducted in a safe environment without disruptions to traffic flow at road intersections.

Constructed in 1960, this bridge is a multiple span structure. Main spans of the structure over US-131 are composed of steel beams while approach spans were constructed using prestressed concrete beams. The bridge spans a total length of 1,035 ft and is 58.4 ft wide (MDOT 2012). Figure 6-15 shows the east side concrete beam approach structure and current condition of Pier 22.



Figure 6-15: Precast Concrete Approach Spans under Franklin Street Bridge.

The bottom concrete deck surface was assigned an overall NBI fair condition rating of 6 during the last inspection on October 23, 2012, however, the degree of deterioration varied between spans and ratings ranged from 5 to 9. These assessment results reflect the overlay of sections in 1990 and, more recently, the replacement of seven concrete deck spans. Replaced deck spans have remained in good condition but other spans contain considerable amounts of spalling and cracking. In addition, soot buildup from locomotive exhaust was reported directly above the railroad line.

6.4.1.1 Ground Truth Information

Prior to the active IR thermography testing, MDOT inspectors used hammer sounding to locate areas of suspected delamination on the underside of the bridge deck on span 22W. The inspectors used spray paint to outline the defect areas. These marked areas were later used to calculate the percentage of deficiency within the test areas and were compared to results of the active IR thermography testing.

6.4.2 Test Locations

From the results of the ground truth testing, three test locations on span 22W of the Franklin Street bridge were selected for the application of active IR thermography to the underside of a concrete bridge deck and pier cap. The lack of surface moisture was used as a primary criteria during the selection process. The selected test locations are described in the following sections and are shown in Figure 6-16.

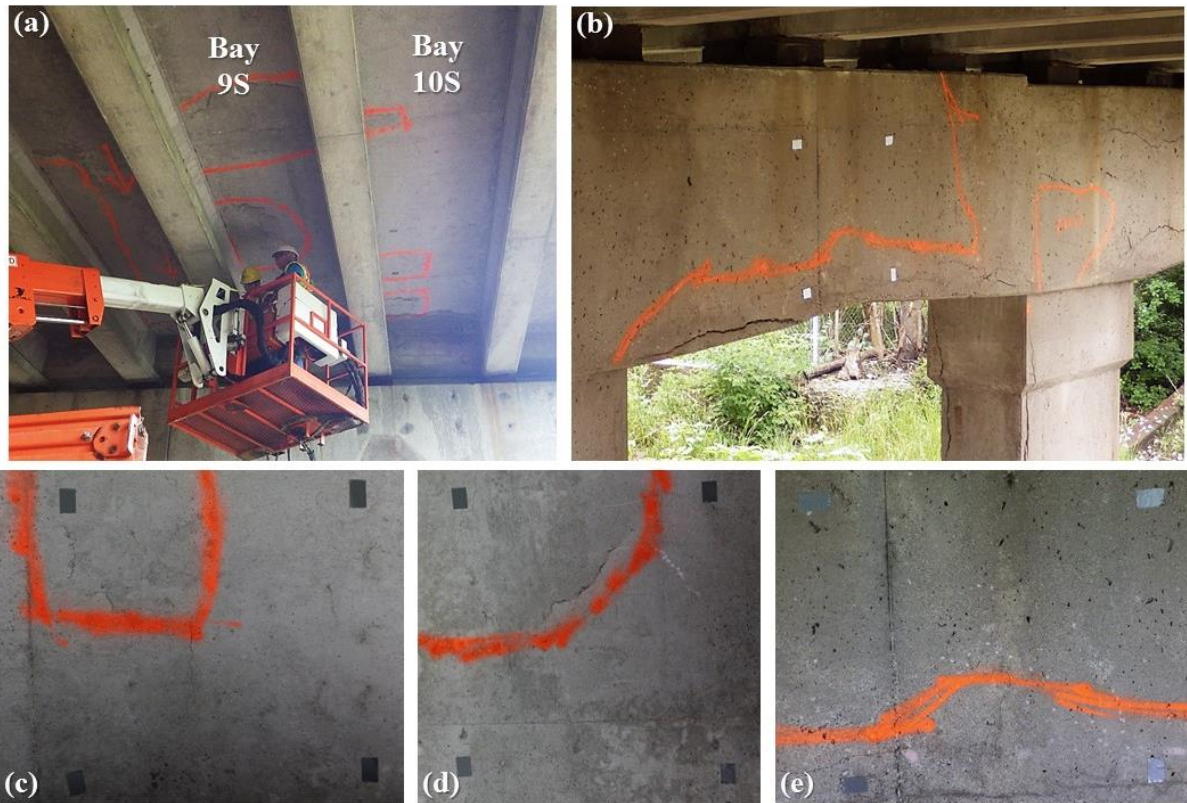


Figure 6-16: (a) Underside of the Franklin Street Bridge Deck. (b) Delamination on Pier 22. (c) Test Location A: Underside of Bridge Deck in Bay 10S. (d) Test Location B: Underside of Bridge Deck in Bay 9S. (e) Test Location C: Pier Cap of Pier 22.

On the scheduled testing day, scattered rain showers and high humidity in the morning had left several areas of the underside of the bridge deck wet due to cracks extending to the top bridge deck and the effects of condensation. These areas were avoided when selecting test locations, as the effects of surface moisture and moisture within concrete can negatively affect results from active IR thermography test methods. Emmissivity is an essential parameter for thermography and can differ for dry concrete and wet concrete. Because of this change in material property, dry concrete may appear at a different temperature in thermal IR images than wet concrete, even if the two areas have the same temperature. Therefore, detecting delaminated areas is more difficult due to the different appearance of wet and dry concrete areas in thermal infrared images.

Rectangular test locations were selected based on the field of view of the thermal infrared cameras used for testing. The corners of all test locations were marked with pieces of tape to visually define the area. The tape aided in aligning the heater, optical image and thermal image prior to data acquisition. The tape marks were also used to correlate and precisely align the optical images with thermal images during analysis procedures. The markers defined an area of approximately 3 ft by 3 ft at each of the test locations.

6.4.2.1 Location A

Test location A was selected for two active IR thermography tests to compare the effects of the duration of the heat impulse on the thermal contrast between areas of delamination and sound concrete and detection of subsurface defects. The first test at this location was conducted using a 15 minute heat time and was identified as test A1. After the heating period, data collection continued for an additional 35 minutes to ensure a majority of the heat impulse had dissipated throughout the concrete and little to no contrast between delamination and sound concrete could be seen in the thermal IR images. A second test was conducted at this location, test A2, using a 5 minute heat time and 25 minute post-heat monitoring time. Laboratory studies have shown that a smaller heat impulse provides less thermal contrast in thermal infrared images. Therefore, data acquisition was terminated sooner than tests conducted with a longer heat pulse because the thermal contrast between delamination and sound concrete diminished sooner. Prior to conducting a test at location A with a 5 minutes heating period, data was acquired at test location B to allow the concrete at location A to reach thermal equilibrium with the ambient environment.

Test location A was located on the far west end of Bay 10S. Ground truth information had revealed that the southwest corner of the selected area contained a suspected delamination. Several surface cracks were observed with a majority located near the suspected delamination. These surface defects were used to align the optical and thermal IR images for analysis.

6.4.2.2 Location B

Test location B was selected for additional active IR thermography testing on the underside of the bridge deck using a heat time of 15 minutes and was identified as test B1. Similar to test A1 conducted at location A, a 35 minute post-heat monitoring time was used to ensure a majority of the heat impulse had dissipated throughout the concrete and little to no contrast between delamination and sound concrete could be seen in the thermal IR images.

Test location B was located on the far west end of Bay 9S. Ground truth information had revealed that the southeast corner of the selected area contained suspected delamination. Several surface cracks were noticed with a majority located near the boundary of the suspected delamination.

6.4.2.3 Location C

One of the objectives of this study was to investigate the feasibility of active IR thermography applied to bridge fascia. Due to the inclement weather on the scheduled testing day, the criteria for selecting a testing location on the bridge fascia beam was not met, however, a testing location on one of the bridge piers was selected instead. The similarity between the test setup for the bridge pier and fascia beam allowed for the evaluation of the active IR thermography testing system on vertically oriented bridge element surfaces.

Test location C was located on the west side of the most southern end of the pier cap at Pier 22. Unlike testing conducted at test location A or B, the heater was positioned vertically to provide the required heat impulse.

6.5 Active Infrared Thermography Field Demonstration Equipment

Two thermal cameras, the high resolution FLIR SC640 used in laboratory studies and a compact lower resolution camera, were used to conduct the tests on the underside of a bridge deck and pier cap. The results from each camera were compared to the ground truth information provided by the Michigan Department of Transportation (MDOT) and the findings were used to make recommendations on the future implementation of active IR thermography for detecting delaminations on bridge superstructure elements not exposed to sunlight. To provide the necessary heat impulse to the selected concrete test areas, the Solaira infrared heater was utilized as the heating effects of this heater were well understood from laboratory investigations. Both the thermal cameras and heater were mounted to the portable support arms fabricated for lab tests. The test equipment and mounting system are shown in Figure 6-17.



Figure 6-17: (A) FLIR SC640 and FLIR Tau 2 Thermal Infrared Cameras (B) Tripod Mounted Solaira Infrared Heater and Thermal Infrared Cameras.

6.5.1 FLIR Tau 2

A FLIR Tau 2 thermal imaging camera was used to investigate the feasibility of using compact, low cost thermal imaging equipment for non-destructive bridge condition assessments. The FLIR Tau 2 is significantly less expensive and smaller than the FLIR SC640 making it more attractive to bridge inspectors and owners. Due to its small size (fitting in the palm of a hand), this camera was mounted directly to the top of the FLIR SC640 in a way to capture a similar test area without obstructing the view of the companion camera.

The FLIR Tau 2 had a 13mm lens and a 336 x 256 pixel display with a 25° x 19° field of view. The camera recorded images to an external memory source where images were later transferred to a computer for analysis procedures. One of the limitations of this thermal camera is that it does not have an external visual display making it difficult to align and determine the appropriate field of view for the test area of interest.

The FLIR Tau 2 was used to record thermal IR images from the time the heater was turned off until termination of the FLIR SC640 data acquisition when a majority of the heat impulse had dissipated throughout the concrete and little to no contrast between delamination and sound concrete could be seen in the thermal IR images shown on the FLIR SC640 visual display. Because analysis procedures used in this study focus on the cooling phase of testing to estimate observation time, the FLIR Tau 2 start time of acquisition was appropriate. The frame rate of the FLIR Tau 2 was correlated to the images acquired from the FLIR SC640 based on the number of images recorded during the duration of the cooling phase of testing.

6.6 Field Demonstration Methodology

To investigate the feasibility of using active IR thermography to detect and quantify delaminations on concrete structural elements of highway bridges, the field test set-up was similar to the developed laboratory test set-up and was used to conduct four tests which are described in detail in the following sections. Using a simplistic area analysis technique and the previously explained absolute contrast analysis method, delaminations were quantified from the results of active IR testing.

6.6.1 Field Application: Test Set-up and Procedure

Several factors dictated the test setup for the active IR thermography field demonstration including the heater size and heater distance. Because the Solaira heater used for testing was relatively small, the test area was limited in size. In addition, the distance from the heater to the concrete surface was established at a distance of 3.5 ft (1.07 m). This distance was used in laboratory studies and was selected to ensure that the heat impulse is capable of producing detectable contrast between delaminations and sound concrete in thermal infrared images over a short period of time (Vaghefi 2013). Increasing the heater distance provides a larger test area and a more uniform heat across the concrete surface for the specific heater used in this test. On the other hand, increasing the heater distance may increase the heat duration needed to obtain the same thermal contrast as closer heater distances. To ensure the thermal infrared cameras captured the heated area on the test location, cameras were positioned 6 ft (1.83 m) from the surface of the test location at an angle of approximately 10° to 20° from normal. This angle was used to get the best perspective of the test area without capturing the image of the heater and was necessary to analyze the relative shapes, locations and depths of delaminations.

To access the underside of the bridge deck and pier cap, MDOT provided a scissor lift truck on the scheduled test date. The hydraulically powered lift platform provided ample space for the tripod mounted heater and cameras as well as a 2000 W generator used to power test equipment. The positioning of the heater and thermal infrared cameras for the pier cap test, as well as the lift truck used to provide access to test locations, can be seen in Figure 6-18.

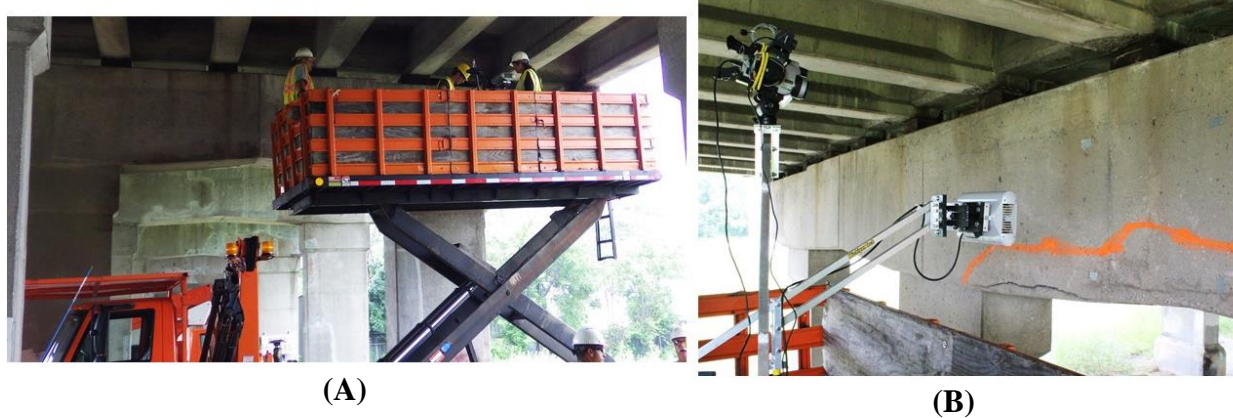


Figure 6-18: (A) Platform Lift Truck (B) Active IR Thermography Test Set-Up for a Franklin Street Bridge Pier Cap.

Prior to active IR thermography testing at each selected location, environmental conditions were measured and used to calibrate the FLIR SC640 thermal imaging camera. A summary of the test numbers and corresponding heat and data acquisition times are shown in Table 6-10. Environmental conditions used for thermal camera calibrations for each test are also summarized in this table.

Table 6-10: Environmental Conditions and Testing Procedure Summary for Field Demonstration Testing.

<i>Test Number</i>	<i>Humidity (%)</i>	<i>Ambient Temperature (°F)</i>	<i>Heat Time (min)</i>	<i>Total Acquisition Time (min)</i>
A1	78.5	75.2	5	30
A2	85.4	71.4	15	50
B1	86.0	71.5	15	50
C1	73.0	76.1	15	50

6.6.2 Data Processing

Two objectives were established for the analysis of data collected during the active IR field demonstration: to estimate the percentage of delamination from thermal images and compare findings to MDOT ground truth information and to investigate the feasibility of estimating delamination depth using a known active IR thermography estimation technique. The following

sections describe the data processing used to complete these objectives and provide an analysis base for future studies.

6.6.2.1 Percent Area of Delamination

To determine the percentage of suspected delaminated concrete area at the three selected test locations on the Franklin Street bridge, and to ensure accurate comparison of ground truth data and the acquired thermal data, the field of view of both the FLIR SC640 and FLIR Tau 2 thermal imaging cameras was correlated to an optical image of the test locations taken from the same perspective as the thermal cameras. Images were aligned using surface features and anomalies such as cracks and spalls, both of which appeared within the thermal images during the heating phase of testing with noticeable contrast from surrounding concrete. This correlation technique was used because the tape markers placed on the concrete surface for image alignment were not consistent with the field of view of the thermal cameras. After correlation, the field of view of the thermal cameras was projected to the optical image generating a total area boundary for comparison.

All processing of the optical images and thermal images was conducted in MATLAB. A simple polygon method was used to determine the percent of delamination on the bridge deck underside and pier cap. No specific polygonal shape was used during analysis, instead, a polygon most similar to the shape of the delamination was constructed. The thermal IR image and optical image correlation of the FLIR SC640 data collected during test B1 as well as the polygon method for determining percent of delamination based on ground truth information can be seen in Figure 6-19. The paint marks placed by MDOT inspectors is seen in Figure 6-19 (B).

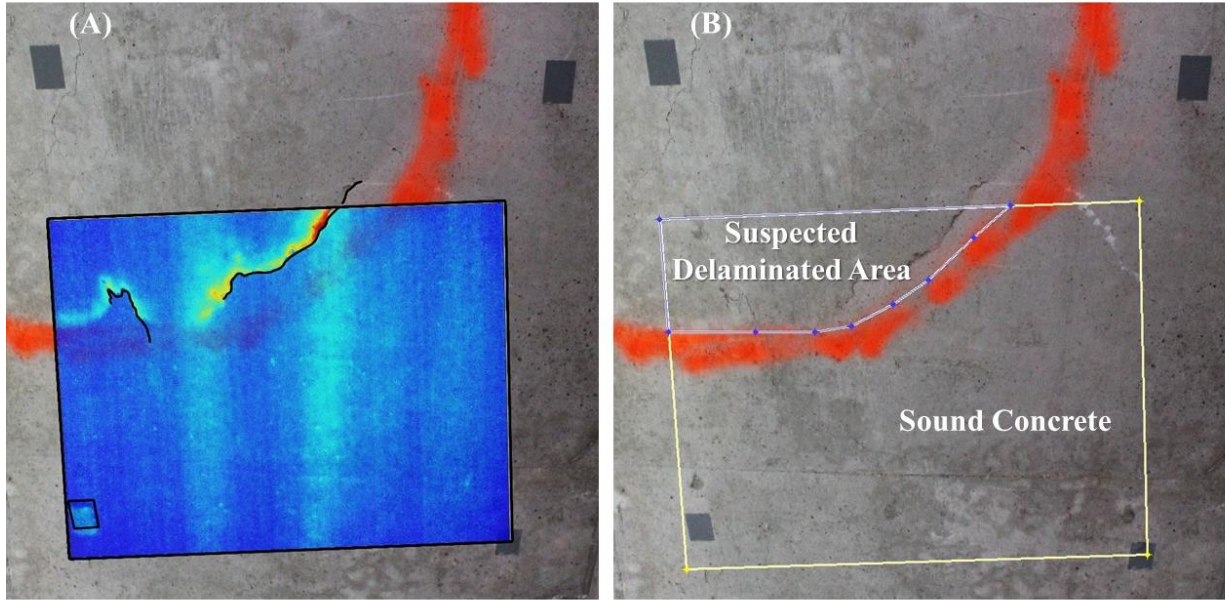


Figure 6-19: (A) Thermal and Optical Image Correlation of FLIR SC640 Using Surface Cracking at Test Location B. (B) Polygon Method for Determining Delamination Percent Based on Ground Truth Information.

The percentage of delaminated area was calculated from the thermal images and optical images using Equation 6-3. The total area of the thermal IR images was taken as the field of view of the corresponding thermal IR camera.

$$\text{Delaminated Area (\%)} = \frac{\text{Number of Pixels of Delaminated Area}}{\text{Number of Pixels of Test Area}} \times 100 \quad \text{Equation 6-3}$$

Within the acquired thermal IR images, delaminations appeared as hotspots compared to surrounding sound concrete. The thermal contrast between the suspected defect and non-defected areas was large enough to process data without image enhancement techniques. At various time intervals, the delamination was subjectively bound by a polygon on the thermal images and Equation 6-3 was used to determine delamination percent. Non-uniform heating, a function of the heater used for testing, did however provide a challenge in bounding the delaminated area on the pier cap, as the contrast between the delamination and thermal heating bands of the heater was difficult to distinguish.

To quantify the ground truth information for thermal image comparison, the simple polygon method was again utilized. Using the projected views from the thermal images as the total area, the suspected delamination marked by MDOT inspectors with spray paint was bounded by a polygon and the percent of delaminated area was calculated using Equation 6-1. For consistency, the polygon was constructed along the inside border of the spray paint closest to the suspected area of delamination.

Both the thermal infrared and optical cameras are recommended to be positioned at a normal angle to the surface of interest to achieve the most accurate results when using the polygon method for determining the percent of delaminated area. Due to the setup of this study and the position of the heater, both the thermal cameras and optical camera were positioned at an angle of approximately 10° - 20° to the test surface. This positioning was adequate for comparing the MDOT ground truth information to the results of active IR thermography because the optical and thermal images were taken at the same perspective to the test locations.

6.6.2.2 Delamination Depth Estimation

To determine the feasibility of using the active IR surface heating method to predict the depth of delaminations on an in-service bridge, depth analysis procedures similar to those developed in laboratory studies were used and are described in earlier sections. All processing of thermal images was conducted in MATLAB. The notable difference between the processing of field data and laboratory data was the selection of a sound concrete background reference area. The background reference area for laboratory studies was selected as a box-shaped polygon surrounding the suspected area of delamination. This analysis shape was selected based on the shape of the simulated Styrofoam delaminations. Due to the geometry and position of delamination in thermal images collected during the field application, a box-shaped polygon could not be used as a reference area. Instead, an L-shape polygon was used as a background reference area. Because the relative shapes of delamination at each selected test location differed, the dimensions and orientation of the L-shaped polygon used during analysis varied. However, a thickness of 5 pixels was used for each of the L-shaped analysis areas for consistency. Figure 6-20 shows the analysis areas selected for a thermal image acquired by the FLIR SC640 during test B1 of the field demonstration.

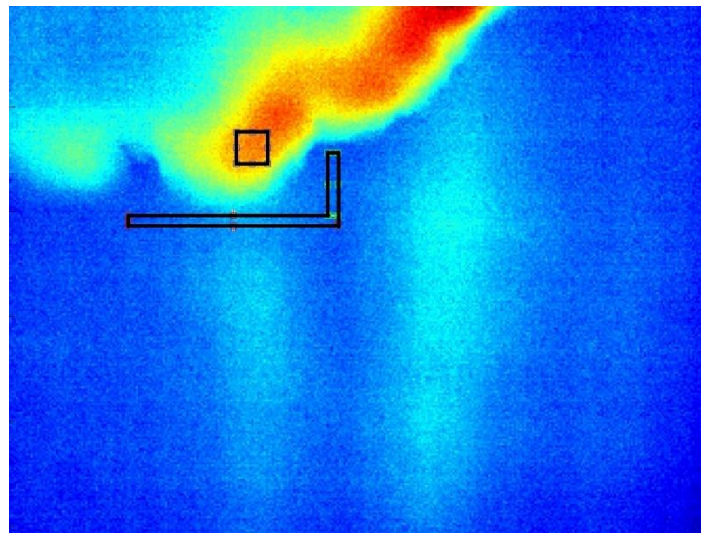


Figure 6-20: Analysis Areas Selected for Test B1 Captured by the FLIR SC640 Thermal Imaging Camera.

Once representative areas of delamination and sound concrete were selected, absolute contrast graphs were constructed. Due to the higher frame rate of the FLIR Tau 2 compared to the FLIR SC640, a moving average of 100 was calculated for this camera to reduce the effects of thermal noise. To determine if depth estimation was feasible, observation times were estimated from each of the absolute contrast plots constructed from data acquired by both thermal cameras used during testing. Because the diffusivity of the concrete used in the construction of the Franklin Street bridge was unknown, delamination depth was not directly estimated, however, previous laboratory studies confirm the relationship between observation time and delamination depth, making this method of determining the feasibility of depth estimation adequate for the objectives of this study (Vaghefi 2013).

6.7 Results and Discussion of Field Demonstration

The following sections present the findings of the field application of active thermography as related to estimation of delamination area and observation times of suspected delaminations at each selected test location on the underside of the bridge deck.

6.7.1 Area of Delamination

Delamination area analysis of the active IR thermography data was based on the visible contrast between delaminated areas and sound concrete in thermal images. For each of the tests conducted, the percent delamination was calculated for both the FLIR SC640 and FLIR Tau 2 every 5 minutes starting at the time the heater was shut off. This time was selected as the starting point of analysis because delaminations are not consistently visible before this point in active IR thermography testing. The maximum percent of delamination for all time step images at each test location is reported in Table 6-11. The data shows that at all testing locations and heat times, the delaminated areas determined by hammer sounding were larger than those detected by active IR thermography. In no test did the area of delamination detected by thermal imaging exceed 83% of hammer sounding results. Thermal images from the FLIR SC640 and FLIR Tau 2 infrared cameras can be seen in Figure 6-21 and include the test number, the maximum detectable delamination size bounded by an analysis polygon, and the acquired time of the thermal IR image from the beginning of the heat time.

It should be noted that the FLIR Tau 2 was not activated during test A1 until 18 minutes after the heater was shut off due to oversight. By the time acquisition initiated, surface anomalies such as spalls and cracking were no longer visible in the thermal images. As a result, the thermal images from the FLIR Tau 2 could not be correlated to the optical image taken at test location A and a total area could not be defined for quantifying ground truth information. The incomplete data is represented by a dash in Table 6-11. However, analysis procedures using the simple polygon method were conducted on the existing set of thermal data recorded by the FLIR Tau 2 during test A1.

Table 6-11: Percent Area Results of Active IR Thermography and Hammer Sounding.

<i>Test Number</i>	<i>Maximum Delamination % by Active IR Thermography (%)</i>	<i>Delamination % by Hammer Sounding (%)</i>	<i>Area of Delamination by Active IR Thermography (ft²)</i>	<i>Area of Delamination by Hammer Sounding (ft²)</i>	<i>% Active IR Area of Hammer Sounding Area (%)</i>	
FLIR SC640	A1	10.91	13.21	0.53	0.64	82.8
	A2	9.71	14.37	0.47	0.70	67.1
	B1	12.67	19.28	0.61	0.93	65.6
	C1	8.08	23.70	0.39	1.15	33.9
FLIR Tau 2	A1	10.37	-	0.62	-	-
	A2	7.92	18.45	0.47	1.10	42.7
	B1	19.02	28.56	1.13	1.70	66.5
	C1	23.47	40.30	1.40	2.40	58.3

- = incomplete data

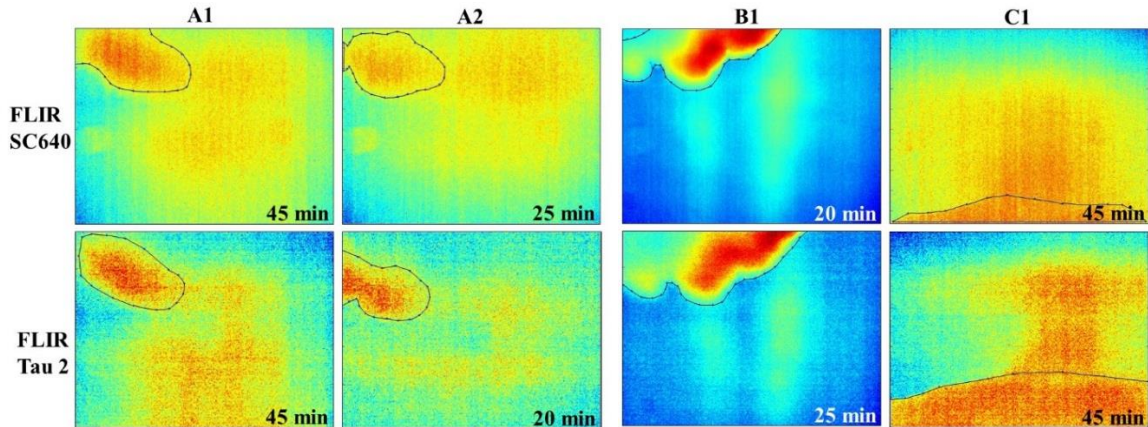


Figure 6-21: Maximum Delamination Areas using Simple Polygon Method for Thermal Image Processing.

While results above indicate hammer sounding predicts larger areas of suspected delamination than with active IR thermography, results also show that several limitations should be considered when detecting and quantifying delamination on concrete elements under a bridge. As previously noted, non-uniform heating adds difficulty to distinguishing the contrast between delaminated areas and areas of sound concrete. Laboratory studies have investigated thermal banding originating from the selected Solaira infrared heater which can be seen in Figure 6-21. For example, vertically oriented heat bands appear in test B1 and horizontal banding appears in test A2. Because of the subjectivity of selecting areas of suspected delamination, thermal banding had a direct effect on the absolute contrast and observation time of delaminations detected at each of the testing locations.

Another limitation to detecting delamination on the underside of a bridge can arise from thermal IR camera functionality. For this field application, two thermal IR cameras, a FLIR SC640 and FLIR Tau 2, were used to collect data. The FLIR SC640 has the ability to be manually focused on a test subject of interest while the FLIR Tau 2 does not contain this function. Because of the uniform temperature of the concrete test areas and the surrounding environment prior to active heating, it became especially difficult to focus the FLIR SC640 on the test areas. Improper focus of the test area may distort the thermal images resulting in less accurate analysis and results. To overcome this limitation, a small object was placed near the surface of the test locations prior to testing. The FLIR SC640 thermal IR camera was focused on this object to ensure image clarity. The object was then removed from the field of view of the camera and testing commenced.

One feature of the FLIR SC640 is that it contains an external display providing a live image to the operator and aiding in alignment of the camera with the test area. Without this ability to produce a live image, the FLIR Tau 2 must be carefully positioned to best capture the test area of interest. This limitation provides challenges for bridge inspectors who cannot be certain of the images they are capturing before post-processing of data. For future applications of active IR thermography, it is recommended that a computer program be developed to display data recorded by the FLIR Tau 2 in real time allowing areas of interest on bridge elements to be captured.

To ensure results from the active IR thermography tests could be compared to MDOT ground truth information, the thermal IR test locations were selected after inspectors completed a delamination survey on span 22W of the Franklin Street bridge. Test locations were selected based on the criteria that they contained areas of delamination and sound concrete areas. Because of this selection criteria and the availability of ground truth information at the time of testing, analysis procedures may have led to the bias detection of delamination.

Although the results of the thermal IR image analysis are subjective for this study and dependent on the operator, data does indicate the presence of similar delaminations at heating times of 15 and 5 minutes during tests A1 and A2. The percent delamination detected by hammer sounding varies for these two tests because the equipment was adjusted between tests causing slight changes in the captured area. Both thermal cameras detected a delamination of lesser area than hammer sounding.

6.7.2 Depth Analysis

To evaluate the performance of Active IR thermography and to investigate the feasibility of using this remote sensing technology to predict the depth of delaminations during field applications, absolute contrast graphs were constructed for all tests using data from both the FLIR SC640 and the FLIR Tau 2 thermal imaging cameras. Figure 6-22 and Figure 6-23 show the absolute contrast graphs from the four tests conducted on the Franklin Street bridge for the FLIR SC640 and FLIR Tau 2 respectively. The end of the heating phase is shown in the FLIR SC640 absolute contrast graphs by a vertical line. Because the FLIR Tau 2 was turned on and

began acquiring data at the end of the heating phase, the absolute contrast graphs for this camera represent only the cooling phase of testing. This starting time of acquisition for the FLIR Tau 2 was adequate for the objectives of this study as the observation time needed for depth analysis is determined from the cooling phase of testing. It should be mentioned again that the FLIR Tau 2 was turned on 18 minutes after the end of the heating phase due to oversight for test A2 and the data collected for this test is shown in Figure 6-23 (B).

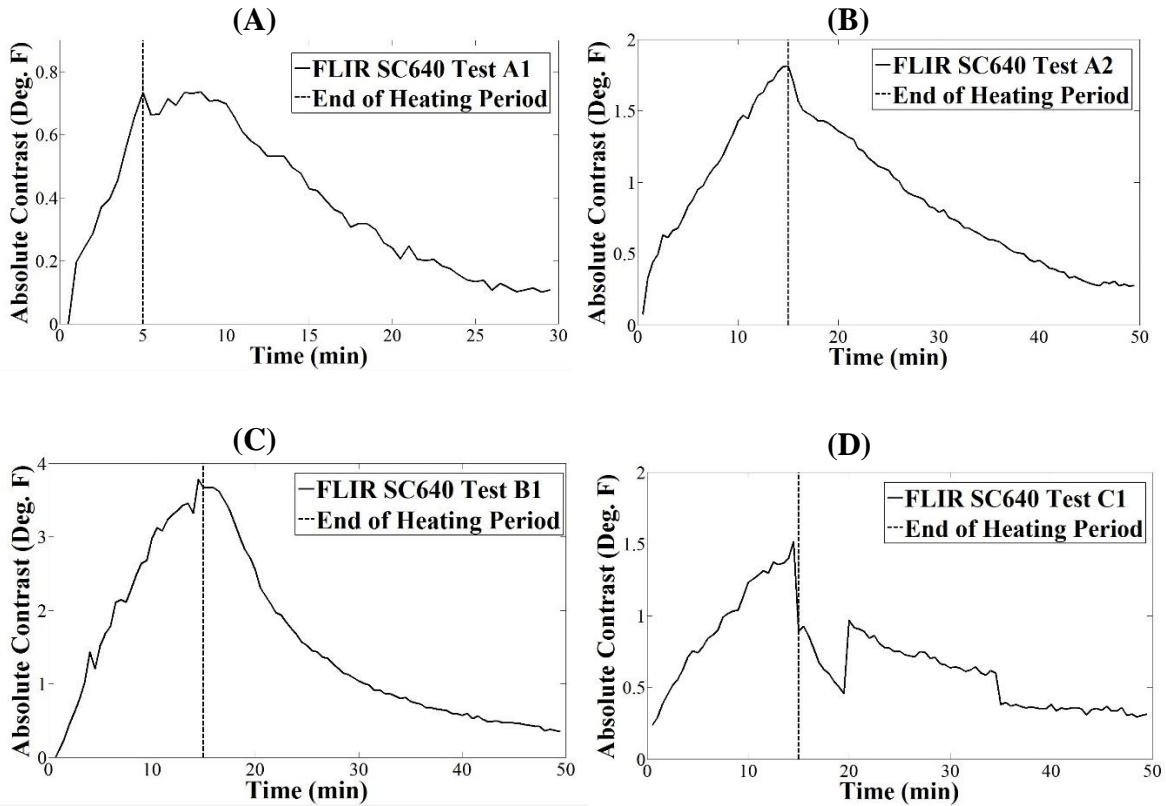


Figure 6-22: FLIR SC640 Absolute Contrast Graphs from Active IR Thermography Field Demonstration Testing (A) Test A1: 5 min. Heat Time (B) Test A2: 15 min. Heat Time (C) Test B1: 15 min. Heat Time (D) Test C1: 15 min. Heat Time.

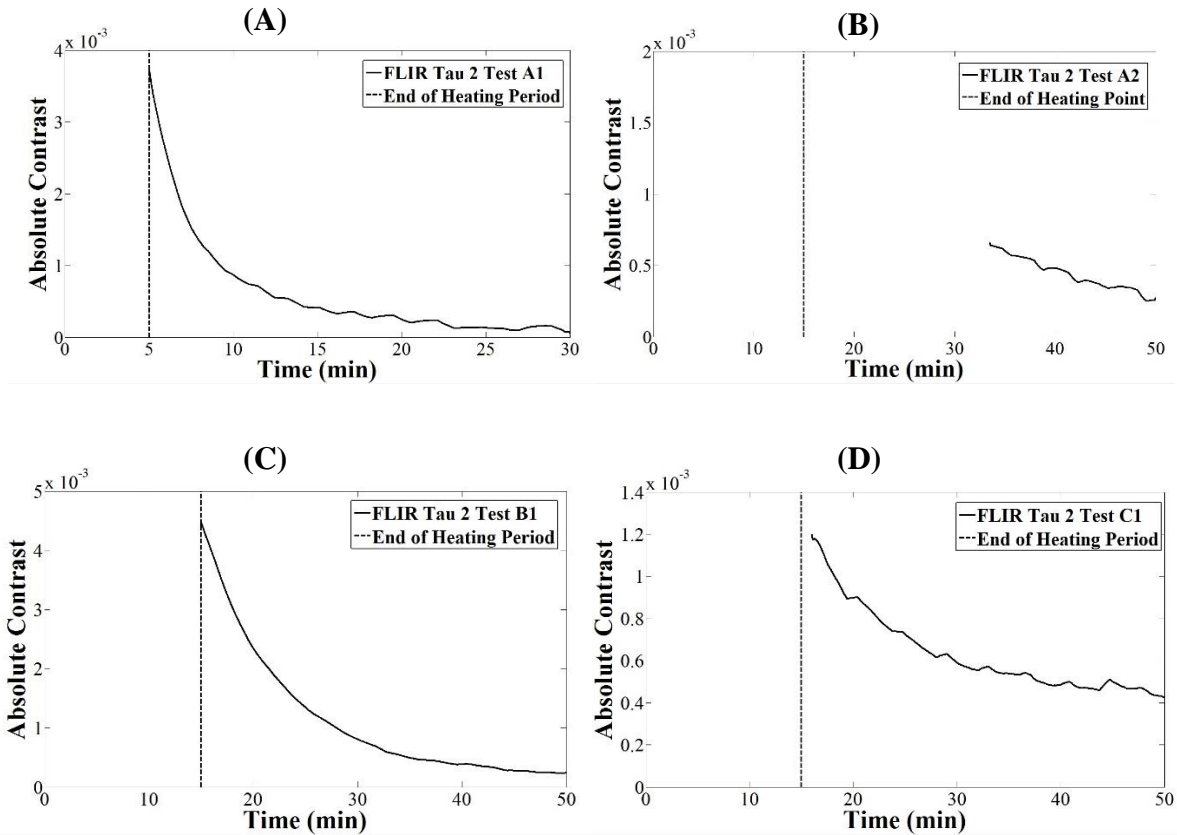


Figure 6-23: FLIR Tau 2 Absolute Contrast Graphs from Active IR Thermography Field Demonstration Testing (A) Test A1: 5 min. Heat Time (B) Test A2: 15 min. Heat Time (C) Test B1: 15 min. Heat Time (D) Test C1: 15 min. Heat Time.

Using the absolute contrast graphs constructed from data captured by both the FLIR SC640 and FLIR Tau 2 thermal cameras, the observation times for the selected delamination reference area were estimated for each test location. The estimated observation time is reported in Table 6-12. Observations of the absolute contrast graphs constructed from FLIR SC640 data show abrupt absolute contrast shifts at 20 min. and 35 min. for test C1 and were shown in Figure 6-22 (D). Due to this erroneous data, observation time could not be determined. To explain these temperature shifts, additional camera functions must be understood. The FLIR SC640 thermal imaging camera contains an internal lens shutter that automatically calibrates the thermal sensor to user defined parameters during data acquisition. It is hypothesized that the thermal camera did not calibrate correctly at 20 min. causing inaccurate shifted temperature readings until a successful calibration at 35 min.

Once observation times for each of the field tests were estimated, the depth of the delamination was estimated using the relationship between observation time, depth squared and thermal diffusivity presented in equation 6-2. The thermal diffusivity, δ , used to calculate depth was estimated from laboratory studies as $0.2219 \text{ in}^2/\text{min}$. It should be noted that this thermal diffusivity value corresponds to the concrete used to construct laboratory test slabs and is likely

different from the concrete used in the construction of the Franklin Street bridge. However, for the objectives and purpose of this study, the estimated diffusivity value is adequate for determining the feasibility of using active IR thermography for delamination depth estimation.

It should also be noted that field data shows delaminations on the bridge deck and pier cap that vary in depth. Variations in thermal contrast between areas above a delamination and areas of sound concrete support this observation. Due to this depth variation, the calculated depth for the field demonstration represents the average depth of the representative delamination area used to construct the absolute contrast graph. While the presented method of analysis allows for delamination depth estimates at relatively small areas, a more robust method should be developed to determine the depth across the entire delamination.

Table 6-12: Estimated Observation Times for Suspected Delaminations on the Franklin Street Bridge Deck and Pier Cap.

	<i>Test Number</i>	<i>Observation Time (min)</i>	<i>Corresponding Absolute Contrast (°F)</i>	<i>Estimated Depth (in)</i>
<i>FLIR SC640</i>	A1	3	0.73	0.82
	A2	6.5	1.3	1.2
	B1	-	-	-
	C1	-	-	-
<i>FLIR Tau 2</i>	A1	-	-	-
	A2	-	-	-
	B1	-	-	-
	C1	-	-	-

Data shows that observation time can be estimated from data collected by the FLIR SC640 thermal camera at test location A from both the 5 min. and 15 min. heat time tests (A1 and A2 respectively). As previously discussed, estimated depth corresponds to the selected analysis areas. For this reason, the depth of the delamination calculated in tests A1 and A2 differ because selected analysis areas are not the same. Observation time could not be estimated using the current analysis techniques in any of the tests conducted at the second bridge deck location or pier cap (tests B1 and C1 respectively). It can also be seen in Table 6-12 that no observation times could be estimated from data acquired by the FLIR Tau 2 thermal camera.

While results from Table 6-12 confirm the use of active IR thermography to estimate the depth of delaminations in concrete bridge elements at test location A, several limitations should be considered when utilizing the described analysis method. Delaminations often form irregular shapes that are variable in depth. As a result, to estimate the depth at any given point of the delamination, the representative area used for absolute contrast calculations is limited in size to ensure a uniform depth in the specified region. The restricted size of the selected delamination

area provides little information about the actual characteristics and dimensions of a large subsurface defect, therefore analysis procedures must be repeated numerous times to quantify the entire delamination. This process may be time consuming and introduce additional interpretation errors due to the subjective nature of the analysis method used in this study. To more efficiently estimate delamination depth in the subsurface of concrete elements, other analysis methods should be further investigated that have automation capabilities allowing for a decreased analysis time.

6.8 Final Conclusions of the Active IR Thermography Inspection

Active IR thermography is a non-destructive condition assessment technique that is gaining popularity among different industries for evaluating and quantifying deterioration of concrete structures due to its simplistic testing and analysis procedures. In addition to remote sensing capabilities, this technology can be used to provide valuable information to inspectors for monitoring delamination growth with time. This study has investigated the potential of applying active IR thermography on concrete bridge elements to assist bridge inspectors in detecting and quantifying delaminations specifically on the underside of concrete bridge decks and piers not exposed to solar heating. The objective of this research was to investigate the feasibility of quantifying delamination area and depth for both laboratory and in-field applications while overcoming some of the limitations of passive infrared thermography. Active IR thermography testing was conducted on several concrete laboratory specimens to develop and provide a base for depth analysis procedures and to investigate several testing parameters. Enhancements to the testing procedure made in the laboratory allowed for the application of this non-destructive testing method on an in-service concrete highway bridge located in downtown Grand Rapids, MI.

Results obtained from initial laboratory testing provide evidence to verify the capabilities of active IR thermography to estimate depth of delaminations in concrete elements using a thermal impulse of 15 minutes using a 1500W heater. Data confirms the linear relationship between the square of the delamination depth and observation time as well as the empirical rule of infrared thermography that delaminations with a width-to-depth ratio greater than 2 and a depth of less than 2 in. from the surface can be accurately detected in thermal images. In addition, testing results demonstrate the effects of delamination size and depth on observation time. Observation time is especially important when selecting an effective time window for acquisition of thermal images to capture delaminations when they appear with maximum contrast to sound areas of concrete.

Completion of parametric laboratory testing revealed several testing variables affecting the thermal contrast between areas of delamination and areas of sound concrete including thermal impulse duration, heater distance from the surface of the concrete test specimen and thermal banding. Decreasing the thermal impulse duration from 15 min. to 5 min. decreased thermal contrast between areas of suspected delamination and areas of sound concrete, however,

delaminations exposed to the shortened impulse were still capable of detection using the selected analysis methods for this study.

One disadvantage of the heating method used in this was non-uniform heating of the concrete test specimens which influenced the selection of analysis areas and determination of observation time from absolute contrast graphs. Non-uniform heating can result from thermal banding originating from heating elements and from heat concentrations produced by decreased heater distances. In either case, selecting representative areas of delamination and sound concrete during analysis procedures becomes increasingly difficult and has a direct effect on absolute contrast. Further investigations are proposed to identify alternative, more appropriate heating sources for future active IR thermography applications.

Advancements to the active IR thermography testing procedure made in the laboratory allowed for testing of several areas on the underside of a concrete highway bridge deck and pier cap located in downtown Grand Rapids, Michigan. The intent of the field application was to address the feasibility of using active IR thermography on concrete bridge elements as a condition assessment method. Results show that active IR thermography is an appropriate non-destructive technique for detecting and quantifying the area of delamination on the underside of bridge decks and is a valuable inspection method for the bridge inspector's toolbox. Test results verify that, unlike passive infrared thermography, active IR thermography is not limited to a specific time window during the day for data collection and can be conducted during a cloudy day as exposure to sun light is not necessary to obtain delamination detection results. In addition, this field application confirms the feasibility of using active IR thermography for condition assessment on vertically oriented concrete bridge elements such as pier caps and the sides of bridge fascia. Furthermore, inclement weather on the test day (including light rain) did not deter data collection as long as tests were conducted in protected areas such as the underside of a bridge deck.

With the use of an external heater to overcome limitations presented by passive IR thermography such as specific testing time windows, active IR thermography can be used for inspection of bridge elements not exposed to the sun. Testing results from the field application show that a heat impulse of 15 min. delivered by the Solaira infrared heater is acceptable for detecting and quantifying subsurface defects. Preliminary results also show that using a shorter heat impulse duration of 5 min. is suitable for quantifying the area of delaminations on the underside of bridge decks and allows for reduced inspection times while using this condition assessment technique. The simplistic analysis method developed to compare MDOT ground truth information to thermal images acquired by the FLIR SC640 and FLIR Tau 2 provide an image processing base for future applications.

In all testing cases, MDOT hammer sounding was at minimum 17.2% greater than delamination areas detected by active IR thermography. Based on the statistics used for comparing hammer sounding to active IR thermography results, it can be concluded that MDOT bridge inspectors are conservative in their condition assessment techniques. However, the limitation of active IR should be considered including the delamination depth and width-to-depth ratio required for

detection using this technology and test set-up. To confirm hammer sounding is more conservative than active IR thermography, advanced thermal image processing should be further investigated. Numerous image enhancement techniques have shown potential to account for non-uniform heating and statistical analysis methods may provide less subjective, automated detection and quantification of subsurface defects.

In addition to determining delamination area using active IR thermography, including the use of reduced heating times, delamination observation times and depths were successfully calculated at test location A on the underside of the bridge deck using concrete thermal diffusivity determined in lab. While many limitations exist for the current depth analysis procedure presented in this chapter, including depth estimation of limited areas, it provides a base for future studies and analysis enhancements.

Results from this field demonstration also address the precision, cost and future capabilities of active IR thermography testing equipment. For all tests conducted on the Franklin Street bridge using both the FLIR SC640 and FLIR Tau 2 thermal cameras, data revealed less delamination per total area than the findings of MDOT inspectors. From these results, it is apparent that less expensive, more portable thermal infrared cameras show promise in detecting delamination area using active IR thermography and should be investigated before further application of this method. With ongoing advancements of technology, thermal cameras are becoming more portable and less expensive with little difference in image quality. Due to the similar performance of the FLIR Tau 2 with the FLIR SC640 in detecting delamination, small, less expensive thermal cameras may provide bridge inspectors with more accurate results than conventional non-destructive condition assessment techniques and allow greater access to bridge elements that cannot be captured using larger size equipment requiring mounting systems. However, the inability of the less expensive camera to focus or provide visual display maybe a deterrent. The field demonstration also confirmed the challenge of evaluating an entire deck underside with a small (3 ft by 3 ft) heating zone, concluding that this technology is most viable to evaluate a small location after an area of concern has been identified.

Furthermore, this research contributes to the current knowledge of the application of active IR thermography for concrete bridge inspection by using the surface heating method. While few previous studies focus on reducing inspection time and the portability of inspection equipment, this study concentrates on the application of active IR thermography to an existing concrete structure with the inspector in mind. Confirming the use of portable infrared heaters and handheld thermal cameras, this study provides evidence that heat times of as little as 5 minutes are capable of providing the necessary heat impulse to detect delaminations. In addition, the estimation of observation times from active IR testing confirms the feasibility of delamination depth estimation in both the laboratory setting and field application and serves as a base for future studies.

7. Project Outreach

Laboratory experiments and field applications of 3DOBS, BVRCS, passive IR thermography and active IR thermography have demonstrated success in the condition assessment of both the top and bottom decks of concrete highway bridges. To provide inspectors and end users the tools and knowledge to use the presented non-destructive remote sensing technologies for effective asset management, several training sessions were provided to MDOT personnel including inspectors, regional engineers, and photogrammetry experts. These training sessions are discussed below.

7.1 MDOT General Training Session

A general training session was conducted in Lansing, Michigan on October 16, 2014 to provide MDOT representatives with an overview of the test methodologies and equipment necessary for the application of each investigated condition assessment technique. With an objective of gaining an understanding of the field readiness and desire of technologies by current bridge inspectors, the three hour session included a presentation conducted by the principal investigators, a hands on equipment demonstration of the 3DOBS, BVRCS and active IR thermography systems and an implementation action plan discussion. The presentation slides from this training session are provided in Appendix G.

The group chose to explore the BVRCS in more depth because of its immediate field readiness, and hence requested an additional session specific to the BVRCS technology. The near highway speed system combining 3DOBS with passive thermography to detect spalls, cracks and suspected delaminations was also critiqued. Likewise, 3DOBS High Resolution system for detecting cracks as small as 1/32 in. was viewed by inspectors as needing guidance from the MDOT photogrammetry office prior to full implementation. A pilot study using the system for several MDOT bridges was suggested as a step towards implementation for scoping and detailed inspections. It was also suggested that the MDOT photogrammetry groups be trained on processing the 3DOBS data so inspectors could begin to use the system.

While the group showed interest in the idea of active thermography for detecting delaminations in areas not exposed to passive heating (sunlight), it was agreed that further study was needed before inspectors could confidently implement the system. Lightweight, portable heating systems, and hand held thermal and optical cameras will be key elements for future successful implementation. Data reduction and analysis methods can be enhanced for inspector use.

As a result of the general training session, two additional training sessions were scheduled to provide more extensive training for MDOT photogrammetry staff to understand the processing of 3DOBS data, and for inspectors to get hands-on experience with the BVRCS Bridgeviewer system, both of which were deemed field ready, deployable technologies.

7.2 Photogrammetry Training Session

A training session was held at the MTRI office in Ann Arbor to show the photogrammetry techniques used for 3DOBS on November 20, 2014. John Lobbestael, Frank Boston, and Calvin Wixtrum from the MDOT photogrammetry department attended. This training session provided a walkthrough of the procedures to create a DEM and Orthoimage of a bridge deck from 3DOBS imagery using Agisoft PhotoScan. A sample dataset taken from a 3DOBS High-Res (Nikon D800) collect was used. Figure 7-1 depicts a general flow of data processing. John Lobbestael and Frank Boston were interested in working together on more application of 3D processing software in transportation. This included other areas of research that MTRI has done for MDOT including the use of UAVs with similar sensors to produce equivalent datasets.

7.3 BVRCS Training Session

A BVRCS training session was conducted at MTRI in Ann Arbor, Michigan on November 20, 2014, and led by MTRI staff members Colin Brooks, David Banach, and Rick Dobson. This session was based on the “BVRCS How To” manual and was presented to MDOT professionals, Eric Burns, Rich Kathrens, Dave Juntunen, and Kay Adefeso. The two-hour training session highlighted BVRCS equipment, use, and data processing methods. Additionally, a live demonstration highlighting how to process data was conducted, including how to link each photo to a GPS coordinate using GeoJot+ and how to hyperlink photos in ESRI ArcGIS Desktop software. The data used for this demonstration was collected during the June 6, 2014 data collection at the Merriman East U-turn Bridge in Livonia, Michigan. During this training session, questions were encouraged and answered. Lastly, a short demonstration on how to place the GoPro cameras on the hood of a vehicle was given outside of MTRI’s office. Each MDOT professional in attendance was given a copy of the BVRCS How To manual, which is included in Appendix H.

At the conclusion of the BVRCS training session, MDOT officials obtained a better understanding into BVRCS equipment, data collection, data processing, and outputs. MDOT discussed potential ways to implement BVRCS equipment (especially the GoPro cameras) into daily bridge inspection methods both on the bridge deck and underneath the bridge. MTRI will potentially aid MDOT with data collection and processing when MDOT fully implements the BVRCS system. It was further suggested by Dave Juntunen that several of these technologies (3DOBS, BridgeGuard and BVRCS) be combined and evaluated on a state-wide basis. This would consist of a pilot study using the system on at least 20 bridges throughout the state to evaluate its ease of use and value added data for MDOT needs.

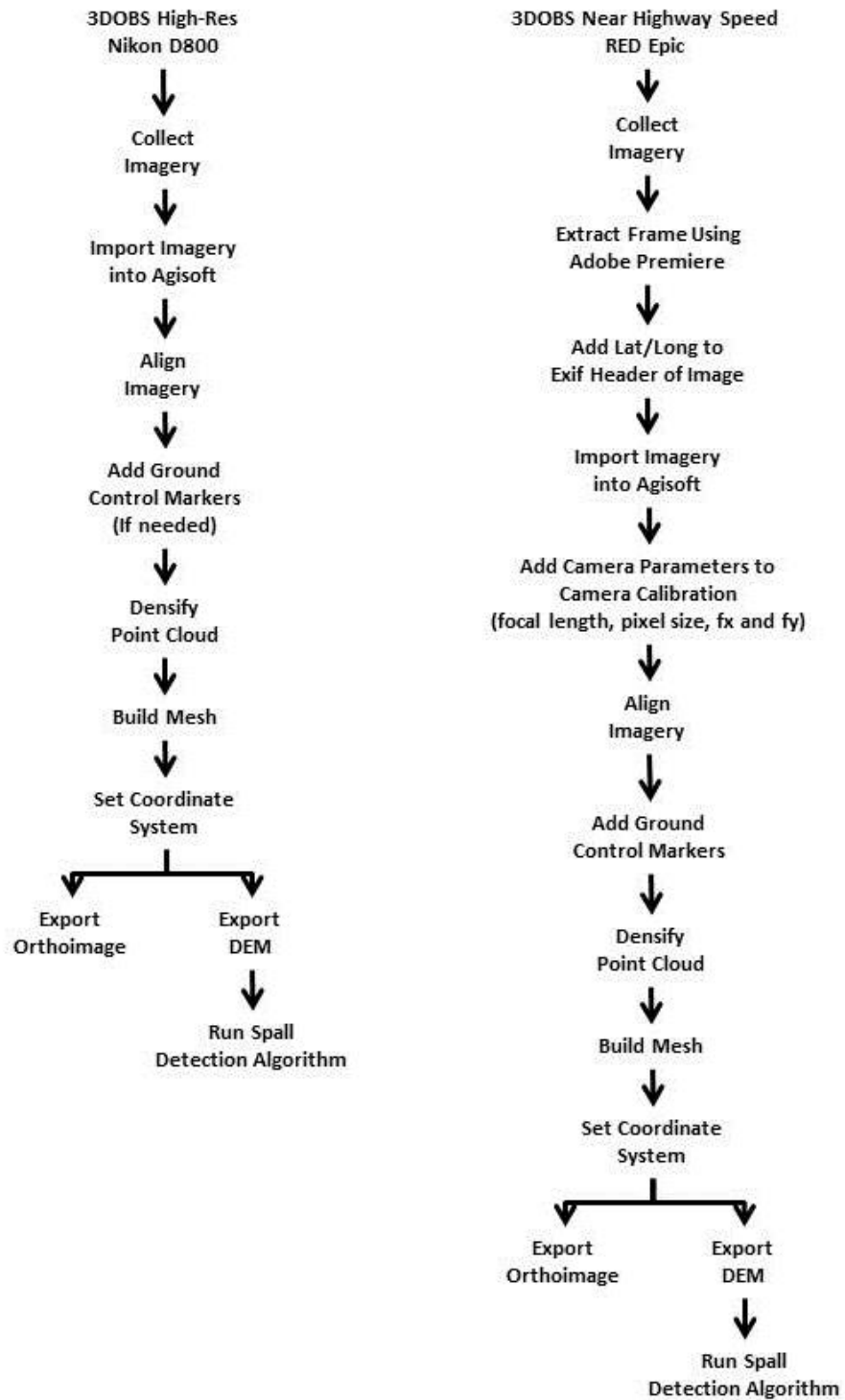


Figure 7-1: Flow Chart Showing the Processing Steps for the High Resolution and Near Highway Speeds Versions of 3DOBS.

8. MDOT NDE Bridge Condition Conclusions

8.1 Conclusions from Study

This research project investigated non-destructive evaluation (NDE) technologies, specifically remote sensing technologies including photogrammetry and thermography, for deployment at near highway speeds to assess the top surface condition of concrete bridge decks. The project also investigated an appropriate remote sensing technology of the evaluation of the underside of the bridge deck. Several non-destructive technologies were upgraded and combined including 3DOBS (3-D Optical Bridge-evaluation System), passive infrared (IR) thermography and BVRCS (BridgeViewer Remote Camera System) onto a single vehicle as an integrated system for condition assessment of the top surface of concrete bridge decks. Integrated data sets can lead to more effective asset management decisions through a more thorough understanding of deck condition. Collection techniques for active IR thermography were also demonstrated on the underside of a bridge deck affording a proof of concept demonstration for the ability to overcome some of the limitations presented with passive IR thermography.

BVRCS has proven to be a low cost, valuable tool for collecting a photo inventory of bridges providing information to inspectors and agencies. The previously implemented system utilizing Canon PowerShot cameras was upgraded to include GoPro cameras that have proved to be more rugged and easier to operate. The deployable system consists of two GoPros, a Garmin GPS and GeoJot+, which can be purchased for a total cost of approximately \$1000. The GeoJot+ software allows for the creation of shapefiles consisting of interpolated points corresponding to the location each photo was captured. Each point is linked to a watermarked version of the collected photo that can be displayed in ArcMap or Google Earth.

The previous deployable 3DOBS system was upgraded into two separate versions to meet the needs of the project requirements to evaluate the top surface of concrete bridge decks: a near highway speed version which is capable of allowing the collection vehicle to travel at speeds up to 45 mph and a high-resolution version capable of detection and classification of cracking to as small as 1/32 in. The RED Epic was chosen for near highway speed collects due to its ability to collect 13.8 MP imagery at up to 60 fps while the Nikon D800 was chosen for high-resolution collects due to its 36.3 MP sensor. Both cameras can be mounted on the same vehicle mount, produce imagery that is processed in Agisoft PhotoScan and can be run through a spall detection algorithm. The tradeoff between the two is speed of the collection vehicle. The RED Epic allows for higher speed at moderate resolution (adequate for spall detection and general crack detection) while the Nikon D800 allows for higher resolution of crack detection at slower speeds.

When 3DOBS was combined with passive IR thermography on the same vehicle mount, both surface and subsurface conditions could be assessed with a single pass per lane. Both datasets were referenced to the same coordinates and could be viewed in GIS such as ArcMap. A total of eight separate data layers are generated from the collected imagery. These layers include an

orthoimage, DEM, hillshade of the DEM, LAS point cloud of the bridge deck, thermal mosaic, detected spalls layer, detected cracks layer, and potential delaminations layer. A combination of these layers would enable MDOT to perform change detection analysis on the distresses and provide objective data to help generate NBI ratings for the bridge deck.

Field demonstrations confirmed that under situations where the bridge deck is in good condition and contains very little or no distresses, it is difficult to reconstruct 3DOBS outputs without additional imagery overlap. For bridges with significant spalls or other features, only a single pass per lane is needed, as there would be enough 3D information in the imagery for accurate reconstruction. For bridge decks without major distress, additional drive-overs may be necessary to properly align imagery for condition evaluation.

Separately, these technologies can provide MDOT with a more detailed understanding of the condition of bridge decks. When combined, these three technologies would ensure MDOT could conduct bridge deck inspections while keeping inspectors safe and away from traffic as well as eliminating the need to close down lanes and passing the time savings onto the traveling public.

Active IR thermography is a non-destructive condition assessment technique with simplistic testing and analysis procedures. This project focused on the application of this technology by using the surface heating method while keeping in mind inspection time and equipment portability. Results obtained from initial laboratory testing verify the capabilities of active IR thermography to detect and estimate depth of delaminations in concrete elements with a width-to-depth ratio greater than 2 and a depth of less than 2 in. using a thermal impulse of 15 minutes and a 1500W infrared heater. In addition, delamination detection using shorter heat times as little as 5 minutes were investigated and confirmed. Lab tests established the need for mounting upgrades prior to field applications resulting in the fabrication of two lightweight, portable mounts for both the heater and camera.

Advancements to the active IR thermography testing procedure made in the laboratory allowed for testing of several areas on the underside of a concrete highway bridge deck and pier cap located in downtown Grand Rapids, Michigan. Two thermal cameras, a high resolution FLIR SC640 and a lower resolution FLIR Tau2, were used to conduct testing as a means of comparison for low-cost equipment. Field deployment showed that this technology overcame limitations presented by passive IR thermography including specific testing time windows, the absence of sun and inability to test in inclement weather. A simplistic analysis method was developed to compare MDOT ground truth information to thermal images acquired by the two thermal cameras, and confirming that MDOT current practice is conservative. Testing results from the field application also showed that a heat impulse of 15 min. is acceptable for detecting and quantifying subsurface defects while using a shorter heat impulse duration of 5 min. is suitable for quantifying the area of delaminations.

Stakeholder input for implementation was gained through several outreach activities. A general training session was held to provide inspectors and end users the tools and knowledge to use the

presented non-destructive remote sensing technologies for effective asset management. Hands-on equipment demonstrations allowed attendees to have one-on-one discussions with researcher on the use, costs and benefits of the technologies. Outcomes included the request for two additional training sessions, one to review the data processing techniques for 3DOBS data with the MDOT photogrammetry group, and one session specifically to demonstrate the use of the BVRCS system for collecting a high-resolution geo-tagged photo inventory of a bridge deck. Training sessions confirmed that bridge inspectors are interested in using advanced technologies for routine, detailed and scoping inspections.

8.2 Recommendations for Further Research

Combining remote sensing technologies to assess the condition of a concrete bridge deck has been shown to be very useful to enhance bridge inspection. As the performance of cameras continues to advance, additional health indicators or condition state will be detectable. It is strongly recommended that MDOT keep abreast of changes in technology through additional interactions with the project team.

Deck cracking is a very real concern to bridge managers. Technology will advance to the point of refined crack detection (to as small as 1/32 in.) at near highway speeds or 1/64 in at slower speeds. Since the start of this project, new DSLRs are being developed with a resolution of 40+ MP and the RED Epic sensor has been upgraded from 13.8 MP to 19.4 MP and capable of 120 fps. These types of upgrades will only increase the ability to detect smaller cracks at faster speeds. Further research needs to include not only the assessment of enhanced camera performance, but also the development of an automated crack detection and classification algorithm. Building from related research would be an important component of automating crack detection. For example, the Transportation Research Board 2015 Annual Meeting has a dedicated poster session on automatic crack detection featuring the work of seven research teams, showing promise that this issue is tractable (see <http://pressamp.trb.org/aminteractiveprogram/EventDetails.aspx?ID=32614>). Similarly, an automated detection algorithm can be developed using thermal imagery to locate potential delaminations, building from current methods focused on analyst interpretation.

Active thermography was investigated as a method to assess the bottom surface condition of a bridge deck. Depth analysis procedures developed in lab were used on data collected in the field and results demonstrate the need for further research to accurately estimate delamination depth. Heating sources to cover larger areas or confined areas should be investigated for use. Thermal cameras range in cost and performance; newer thermal cameras can be 1/10 the cost of ones purchased five years ago. This study used systems that were currently available for proof of concept testing and did not consider camera performance. Results of several cameras should be compared to determine the best equipment.

The use of unmanned aerial vehicles (UAVs) for condition assessment has a growing popularity. Remote sensing technologies, including optical, thermal, and LiDAR, have been successfully

demonstrated to MDOT through other research opportunities (“Evaluating the Use of Unmanned Aerial Vehicles for Transportation Purposes”, 2013-067, No. 1, OR13-008, led by PI C.Brooks). Combining UAVs with the data fusion and common platform for technologies can enhance inspection for bridge decks, superstructures, and other transportation infrastructure. Pilot studies are recommended to demonstrate the optimal use of UAVs for condition assessment of bridge decks, in relation to vehicle-based and manual assessment, building from MDOT’s recent research investment in this area.

As experts in remote sensing applications for transportation infrastructure, the project team is available to assist MDOT with their future research needs in an area of rapidly changing technology. Data processing techniques for assessment of a variety of health indicators are yet to be developed and can be applied to a host of situations including evaluation of steel and timber superstructures and substructures. Future research could address these additional bridge types and construction materials.

8.3 Recommendations for Implementation

An Implementation and Action Plan has been drafted to direct the Research Advisory Panel and other MDOT personnel in the steps necessary to implement the results of the research program. The draft plan is included in Appendix I. Data collection at near highway speed for the top of deck condition assessment and proof of concept testing for the underside of the deck was conducted for surface and subsurface evaluation. Recommendations are included for combining multiple remote sensing technologies into a single vehicle delivery. This section summarizes the implementation action plan.

The BridgeViewer BVRCS, a system shown to provide high resolution imagery using GoPro cameras to discern spalls and patchwork on a concrete deck while traveling at 45 mph and above, is near ready for deployment. The system is commercially available and low cost (less than \$1000) , and can provide an assessment method comparable to visual inspection in a very short time. A hands-on demonstration session was provided for bridge inspectors and managers to begin implementation. It is recommended that MDOT begin with introducing the system into one region for all upcoming inspections. Inspectors will quickly learn the system operation and gain the benefit of having a high-resolution geo-tagged photo inventory of the bridge deck collected while travelling at highway speed without traffic interruption.

Top of deck evaluation at near highway speed can also include the detection of spalls, cracking, and suspected delaminations by combining 3-D photogrammetry and thermography data collections. A total of eight separate data layers generated from the collected imagery can assess the surface and subsurface condition of the deck. Imagery captured at near highway speed (45 mph) can detect spalls and delaminations, while imagery captured at slower speeds with higher resolution cameras can detect cracking to 1/32 in. It is recommended that these remote sensing technologies be integrated to the bridge inspector’s suite of tools for inspection. Capital

investment in equipment, training of inspectors, and coordination with the MDOT photogrammetry office are necessary for implementation.

Common to the implementation of all these technologies, is the tough question that MDOT must assess thoroughly to fully understand the path to implementation. How will this data be used? Strategic discussions are needed within MDOT bridge management groups to explore the best strategies to utilize the data, such as whether time-history data can be used through a decision support system to predict service life for alignment of maintenance and repair funds, or how this information can be used to enhance the bridge preservation program. Pilot studies with an increased sample population will add confidence in the data and methodology for providing valuable information about the condition state of the concrete bridge deck.

Further development of the active thermography method is necessary prior to implementation for use in bridge inspection of concrete bridge decks. Studies should include variable heat sources and heating times for inspector convenience while optimizing data collection. Methods of analysis have been simplified, and upgraded equipment with improved resolution and lower costs should be considered. Most important, MDOT must decide where and when is the most appropriate use of the technology. While the method was demonstrated here for the bottom surface of a concrete bridge deck, any location where there is little to no solar heating may benefit from the use of active thermography.

MDOT is a leader in cutting edge research for enhancing bridge inspection. Proof of concept testing and field demonstrations for remote sensing technologies are necessary steps in the implementation of new systems and methodologies.

References

- AASHTO (2011). AASHTO Guide Manual for Bridge Element Inspection. First Edition, American Association of State Highway and Transportation Officials.
- AASHTO. (2008). "Bridging the Gap: Restoring and Rebuilding the Nation's bridges." Retrieved April, 2013, from <ftp://ftp.mdt.mt.gov/research/LIBRARY/BTG-1-BRIDGING-GAP-AASHTO.PDF>.
- Abdel-Qader, I., S. Yohali, O. Abudayyeh and S. Yehia (2008). "Segmentation of thermal images for non-destructive evaluation of bridge decks." NDT & E International **41**: 395-405.
- Abdel-Qader, I., S. Yohali, O. Abudayyeh and S. Yehia, 2008. "Segmentation of Thermal Images for Non-Destructive Evaluation of Bridge Decks." *NDT & E International*, 41, pp. 395-405.
- ACI (2001). Protection of Metals in Concrete against Corrosion (ACI 222R). Farmington Hills, MI, American Concrete Institute.
- Ahlborn, T. M., R. Shuchman, L. L. Sutter, D. K. Harris, C. N. Brooks and J. W. Burns (2012). Bridge condition assessment using remote sensors. Final project report, USDOT/RITA. Cooperative agreement # DTOS59-10-H-00001.
- Arndt, R. W., 2010. "Square Pulse Thermography in Frequency Domain as Adaption of Pulsed Phase Thermography for Qualitative and Quantitative Applications in Cultural Heritage and Civil Engineering." *Infrared Physics and Technology*, 53, pp. 246-253.
- ASTM (1997). ASTM D 4580 - 86: Standard Practice for Measuring Delaminations in Concrete Bridge Decks by Sounding, American Society of Testing Materials.
- ASTM (2007). ASTM D4788-03: Standard test method for detecting delaminations in bridge decks using infrared thermography, American Society of Testing Materials.
- ASTM, 2007, ASTM D4788-03: Standard Test Method for Detecting Delaminations in Bridge Decks using Infrared Thermography, American Society of Testing Materials.
- Brown, J. R. and H. R. Hamilton, 2007. "Heating Methods and Detection Limits for Infrared Thermography Inspection of Fiber-Reinforced Polymer Composites." *ACI Material Journal*, 104(5), pp. 481-490.
- Clark, M. R., D.M. McCann and M. C. Forde (2003). "Application of Infrared thermography to the non-destructive testing of concrete and masonry bridges." NDT & E International **36**: 265-275.
- Engineering ToolBox. 2012. "Thermal Conductivity of Some Common Material and Gases." Retrieved October 30th, 2012 from <http://www.engineeringtoolbox.com/thermal->

[conductivity-d_429.html](#).

- Federal Highway Administration (FHWA) (2006). Bridge Inspector's Reference Manual (BIRM). Washington, D.C.
- FHWA (2006). Bridge Inspector's Reference Manual (BIRM). Washington, D.C., Federal Highway Administration.
- FHWA. (2011). "National Bridge Inventory (NBI)." 2013, from <http://www.fhwa.dot.gov/bridge/nbi/deck.cfm>.
- FHWA Bridge Preservation Guide, 2011. US Department of Transportation. Report No. FHWA-HIF-11042, McLean, VA.
- Fu, G., Ed. (2005). Inspection and monitoring techniques for bridges and civil structures. Cambridge, England, Woodhead Publishing in Materials.
- Ghosh, K. K. and V. M. Karbhari, 2006. "A Critical Review of Infrared Thermography as a Method for Non-Destructive Evaluation of FRP Rehabilitated Structures." *International Journal of Materials and Product Technology*, 25(4), pp. 241-266.
- Gucunski, N., A. Imani, F. Romero, S. Nazarian, D. Yuan, H. Wiggenhauser, P. Shokouhi, A. Taffe and D. Kutrubes (2013). Nondestructive testing to identify concrete bridge deck deterioration. SHRP2. Washington, D.C.
- Halabe, U. B., H. V. S. GangaRao and N. Perisetty, 2012, Infrared Thermography and GPR Techniques for Condition Assessment of RC Bridges. *NDT/NDE for Highways and Bridges: Structural Materials Technology (SMT)*. New York City, NY.
- Henriksen, S., Ed. (1994). The glossary of mapping sciences. New York, NY, American Society of Civil Engineers.
- Howard, G. B. and C. P. Sturos (March 2010). Data at Speed. Roads and Bridges. Howard, G. B., C. P. Sturos and T. M. Ahlborn (Feb 2010). On the fly over. Roads and Bridges.
- Jana, D. (2007). Delamination - A State of The Art Review. Proceedings of the Twenty- Ninth Conference on Cement Microscopy Quebec City, PQ, Canada.
- Jenson, J. (2007). Remote sensing of the environment: an earth resource perspective, Pearson Education, Inc. Jiang, R., D. V. Ja'uregui and K. R. White (2008). "Close-range Photogrammetry Applications in Bridge Measurement: Literature review." Measurement **41**(8): 823-834.
- Kurita, K., M. Oyado, H. Tanaka and S. Tottori, 2009. "Active Infrared Thermographic Inspection Technique for Elevated Concrete Structures using Remote Heating System." *Infrared Physics and Technology*, 52, pp. 208-213.
- Lamond, J. F. and J. H. Pielert, Eds., 2006. *Significance of Test and Properties of Concrete and Concrete-Making Materials*. STP-169d. Bridgeport, NJ, ASTM International.

- Levar, J. M. and H. R. Hamilton, 2003. "Nondestructive Evaluation of Carbon Fiber-Reinforced Polymer-Concrete Bond using Infrared Thermography." *ACI Material Journal*, 100(1), pp. 63-72.
- Maas, H.-G. and U. Hampel (2006). "Photogrammetric techniques in civil engineering material testing and structure monitoring." *Photogrammetric Engineering and Remote Sensing* **72**(1): 7.
- Maierhofer, C., A. Brink, M. Rolling and H. Wiggenshauser, 2002. "Transient Thermography for Structural Investigation of Concrete and Composites in the Near Surface Region." *Infrared Physics and Technology*, 43, pp. 271-278.
- Maldague, X. P. V. (1993). Nondestructive evaluation of materials by infrared thermography. London, Springer-Verlag.
- Maldague, X. P. V. and P.O. Moore, 2001, *Nondestructive Testing Handbook: Infrared and Thermal Testing*, American Society of Nondestructive Testing.
- Maldague, X.P.V., 1993, *Nondestructive Evaluation of Materials by Infrared Thermography*, London, Springer-Verlag.
- McGlone, J. C., E. M. Mikhail, J. S. Bethel and R. Mullen, Eds. (2004). Manual of Photogrammetry. Bethesda, MD, American Society for Photogrammetry and Remote Sensing.
- MDOT, 2003, Standard Specifications for Construction. Lansing, MI, Michigan Department of Transportation.
- MDOT. (2007). "Pontis Bridge Inspection Manual." Retrieved January, 2013, from http://www.michigan.gov/documents/mdot/MDOT_BridgeDeckMatrix_withUncoatedBlackRebar_355077_7.pdf.
- MDOT. (2008). "Bridge Deck Preservation Matrix." Retrieved July, 2012, from http://www.michigan.gov/documents/mdot/MDOT_BridgeDeckMatrix_withUncoatedBlackRebar_355077_7.pdf.
- MDOT. (2009). "Project Scoping Manual." Retrieved July, 2012, from mdotwas1.mdot.state.mi.us/public/docs/scoping/Scoping_Manual.pdf.
- MDOT. (2011). "Bridge Deck Preservation Matrix." Retrieved July, 2012, from http://www.michigan.gov/documents/mdot/MDOT_BridgeDeckMatrix_withUncoatedBlackRebar_355077_7.pdf.
- MDOT. (2011). "Bridge Safety Inspection NBI Rating Guidelines." Retrieved January, 2013, from http://www.michigan.gov/documents/mdot/MDOT_BIR_Ratings_Guide_367482_7.pdf.

- MDOT. 2008. "Bridge Deck Preservation Matrix." Retrieved July, 2012, from www.michigan.gov/documents/mdot/MDOT_BridgeDeckMatrix_withEpoxyCoatedRebar_355086_7.pdf.
- MDOT. 2012. "Bridge Management and Inspection System." Retrieved May 2014 from <http://mdotjboss.state.mi.us/mbrs/bridgeDashboard.do#no-back-button>.
- Moore, M., B. Phares, B. Graybeal, D. Rolander and G. Washer (2000). Reliability of visual inspection for highway bridges, NDE Validation Center/FHWA.
- Pollock, D. G., K. J. Dupuis, B. Lacour and K. R. Olsen (2008). Detection of Voids in Prestressed Concrete Bridges using Thermal Imaging and Ground Penetrating Radar, Washington State University.
- Ryan, T. W., R. A. Hartle, J. Eric Mann and L. J. Danovich (2006). Bridge Inspector's Reference Manual. Washington D.C., FHWA.
- Spring, R., R. Huff and M. Schwoegler (2011). "Infrared Thermography: A Versatile Nondestructive Testing Technique." *Materials Evaluation* **69**(8): 935-942.
- Starnes, M. A. (2002). Development of technical bases for using infrared thermography for nondestructive evaluation of fiber reinforced polymer composites bonded to concrete. *Civil and Environmental Engineering*, Massachusetts Institute of Technology.
- Starnes, M. A., N. J. Carino and E. A. Kausel, 2003. "Preliminary Thermography Studies for Quality Control of Concrete Structures Strengthened with Fiber-Reinforced Polymer Composites." *ASCE Journal of Materials in Civil Engineering*, 15(3), pp. 266-273.
- Vaghefi, K. and T. M. Ahlborn, 2013. "Application of Active Infrared Thermography for Inspecting Existing Concrete Structures." *NDT & E International*, In review since October 2013.
- Vaghefi, K., 2013, Infrared Thermography Enhancements for Concrete Bridge Evaluation. *Civil and Environmental Engineering*, Michigan Technological University. Ph.D.
- Vaghefi, K., R. C. Oats, D. K. Harris, T. M. Ahlborn, 2011, Application of Thermal IR Imagery for Concrete Bridge Inspection. *PCI Convention and National Bridge Conference*. Salt Lake City, Utah, Prestressed/Precast Concrete Institute.
- Vaghefi, K., R. C. Oats, D. K. Harris, T. M. Ahlborn, C. N. Brooks, K. Endsley, C. Roussi, R. Shuchman, J. W. Burns and R. Dobson (2012). "Evaluation of Commercially Available Remote Sensors for Highway Bridge Condition Assessment." *ASCE Journal of Bridge Engineering* **17**(6): 886-895.
- Vaghefi, K., T. M. Ahlborn, D. K. Harris and C. N. Brooks (2013). "Combined Imaging Technologies for Concrete Bridge Deck Condition Assessment." *ASCE Journal of Performance of Constructed Facilities* Accepted April 2013.

Washer, G. (2010). Thermal Imaging of Damage in Bridge Soffits. NDE/NDT for Highways and Bridges: Structural Materials Technology, NYC.

Washer, G., R. Fenwick and N. Bolleni (2009 a). Development of hand-held thermographic inspection technologies. OR10-007.

Washer, G., R. Fenwick, N. Bolleni and J. Harper (2009 b). "Effects of environmental variable on infrared imaging subsurface features of concrete bridges." Journal of the transportation research board No. 2108: 107-114.